

**DEVELOPMENT OF A NON-INTRUSIVE CONTINUOUS SENSOR FOR
EARLY DETECTION OF FOULING IN COMMERCIAL
MANUFACTURING SYSTEMS**

by

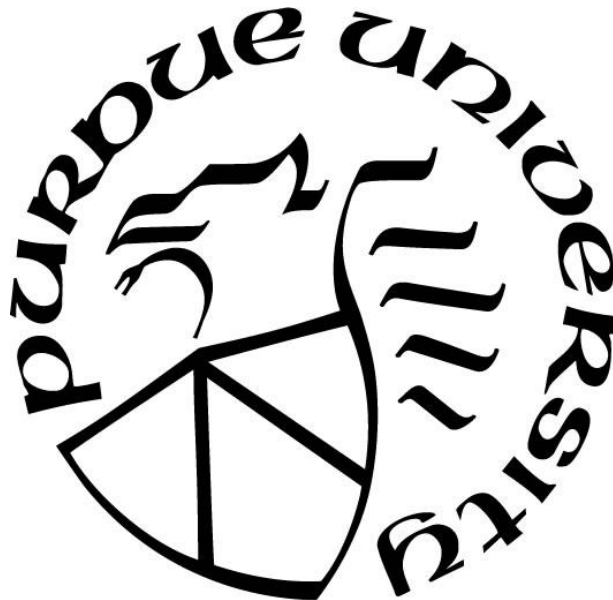
Fernando José Cantarero Rivera

A Thesis

Submitted to the Faculty of Purdue University

In Partial Fulfillment of the Requirements for the degree of

Master of Science



Department of Food Science

West Lafayette, Indiana

August 2020

**THE PURDUE UNIVERSITY GRADUATE SCHOOL
STATEMENT OF COMMITTEE APPROVAL**

Dr. Dharmendra K Mishra, Chair

Department of Food Science

Dr. Jen-Yi Huang

Department of Food Science

Dr. Ferhan Ozadali

Global R&D and Engineering Director, Reckitt Benckiser Group

Approved by:

Dr. Arun Bhunia

Dedicated to my family (Manuel, Miriam, and Carlos) and friends for their endless support during the development of this project.

ACKNOWLEDGMENTS

I would like to acknowledge:

- Ferhan Ozadali for helping us obtain a considerable amount of HWC to be able to process.
- Jen-Yi Huang for helping understand all things related to fouling.
- Dharmendra Mishra and lab mates for guidance and support.
- Rhonda Taylor for always keeping me positive and pushing forward.
- Erik Kurdelak for the unmeasurable amount of help provided to set up experiments and processing knowledge passed on.

TABLE OF CONTENTS

LIST OF TABLES	7
LIST OF FIGURES	8
NOMENCLATURE	10
ABSTRACT.....	12
CHAPTER 1. INTRODUCTION	14
CHAPTER 2. LITERATURE REVIEW	18
2.1 Aseptic Processing of Foods.....	18
2.2 Fouling	19
2.2.1 Types of Fouling.....	19
2.2.2 Methods for Fouling Detection.....	20
2.3 Thermal Properties of Foods.....	22
2.4 Parameter Estimation and Inverse Problems	24
2.4.1 Scaled Sensitivity Coefficients	24
2.4.2 Sequential Estimation	25
2.4.3 Parameter Estimation in Food Science	26
CHAPTER 3. MATERIALS AND METHODS.....	27
3.1 Product Description and Equipment Design.....	27
3.1.1 Description of Data Acquisition	28
3.2 Mathematical model.....	29
3.2.1 Sensor Design	29
3.2.2 Fouling layer model.....	33
3.3 Instrument calibration	37
3.4 Scaled Sensitivity Coefficients	37
3.5 Optimal Experimental Design.....	38
3.6 Sequential Estimation	39
CHAPTER 4. Results and Discussion.....	41
4.1 Instrument Calibration	41
4.2 Scaled Sensitivity Coefficients	41
4.3 Optimal Experimental Design.....	43

4.4	Sequential Estimation of Thermal Conductivity.....	45
4.4.1	Sensor Calibration	45
4.4.2	Fouling Layer Thermal Conductivity Estimation.....	49
4.5	Fouling Layer Image Analysis.....	57
CHAPTER 5.	CONCLUSIONS and Future Work	60
APPENDIX A.	Typical Raw Experimental Data File	62
REFERENCES	65

LIST OF TABLES

Table 2.1. Typical UHT sterilization processes.....	18
Table 2.2. Comparison of different detection methods together with their advantages and limitations.	20
Table 2.3. Classification of techniques to monitor fouling or product changes – Scientific or Industrial application (Sc/Ind), batch or continuous process (B/C), local or global measurements (L/G), intrusive or non-intrusive sensors (In/N-In), On-line or Post-Process (OL/PP) and Direct or Indirect thickness estimation (D/Ind).....	21
Table 2.4. Thermal property models for food components ($-40 \leq t \leq 300$ °F).....	23
Table 3.1. Material properties used in COMSOL models.	36
Table 4.1. Mean estimated thermal conductivities for all products and their corresponding 95% confidence interval (CI).....	47
Table 4.2. Average thickness and thermal resistance of the fouling layer for HWC and 15% NFDM	59

LIST OF FIGURES

Figure 2.1. SEM imaging of fouling. (a) Type B fouling, CaCO ₃ deposits. (b) Type A fouling, protein, and carbohydrate complex. Figure from (Thamaraiselvan & Noel, 2015)	20
Figure 3.1. Process flow diagram for the MicroThermics 25-HV HTST/UHT lab scale unit used in study.....	27
Figure 3.2. Sketch of NICS mounting on MicroThermics® unit.	28
Figure 3.3. Simulated heating (red = hottest) and flow (arrow size is indicative of velocity magnitude) profile of NICS.	30
Figure 3.4. Fully developed laminar flow profile of NICS. (Arrow size is indicative of velocity magnitude)	31
Figure 3.5. Model geometry highlighting fouling layer	34
Figure 3.6. Model mesh quality (skewness) evaluation.....	36
Figure 4.1. Voltage input and power calibration curve for NICS heater.	41
Figure 4.2. Scaled sensitivity coefficient (SSC) for estimation of the thermal conductivity of Glycerol at room temperature.	42
Figure 4.3. Delta values obtained for different time-power (pulse) profiles for heater in NICS... ..	43
Figure 4.4. Temperature profile of a 10% NFDM trial showing the heat generated by the sensor.	44
Figure 4.5. Residual plot for a 10% NFDM trial showing difference between experimental and predicted data.	45
Figure 4.6. Thermal conductivity of Glycerol updated at every new data point.	46
Figure 4.7. Box-and-whisker plot showing the variability of the estimated thermal conductivities for the products used in the study.	47
Figure 4.8. All experiments for one HWC trial plotted on a same scale to locate variances and estimate h accordingly.	50
Figure 4.9. Scaled sensitivity coefficient (SSC) for estimation of the thermal conductivity of HWC at 140 °C.	51
Figure 4.10. Percentage of the change in temperature represented by the SSC at each data point for HWC	52
Figure 4.11. Percentage of the change in temperature represented by the SSC at each data point for NFDM.	53
Figure 4.12. Temperature profile for the sensor heat pulse at 15 and 60 minutes of processing HWC.	54

Figure 4.13. Residual plots for HWC temperature profile at 15 and 60 minutes of processing... 54

Figure 4.14. Estimated k average with 95% confidence interval for NFDM trials. 56

Figure 4.15. Estimated k average with 95% confidence interval for HWC trials. 56

Figure 4.16. Photo of a fouled tube section mounted with NICS after (a) HWC trial and (b) NFDM trial 57

Figure 4.17.(a) ROI lines measuring pixels and scaling factor window (b) ROI lines measurements converted into corresponding units. 58

NOMENCLATURE

A	Inversion matrix ($p \times m$)
b	Parameter vector
b^*	Estimated parameter vector
C	Specific heat (kJ/(kg·K))
C_a	Specific heat of air (kJ/(kg·K))
C_f	Specific heat of fouling layer (kJ/(kg·K))
C_h	Specific heat of heater (kJ/(kg·K))
C_p	Specific heat of product (kJ/(kg·K))
C_{ss}	Specific heat of stainless steel (kJ/(kg·K))
e	residuals, error vector
F	Volumetric forces tensor (N/m ³)
h	Heat transfer coefficient (W/m ² ·K)
I	Identity matrix
K	Average viscous stress tensor (Pa)
K_{i+1}	Gain matrix
k	Thermal conductivity (W/(m·K))
k_a	Thermal conductivity of air (W/(m·K))
k_f	Thermal conductivity of fouling layer (W/(m·K))
k_h	Thermal conductivity of heater (W/(m·K))
k_p	Thermal conductivity of product (W/(m·K))
k_{ss}	Thermal conductivity of stainless steel (W/(m·K))
m	Observations at given time
n	Kinematic viscosity (m ² /s)
n	Number of data
P	Covariance matrix ($p \times p$)
p	Number of parameters
Q	Volumetric heat source (W/m ³)
q	Heat flux (W/m ²)
q_0	Convective heat flux (W/m ²)
R_f	Resistance of fouling layer in (m ² ·K)/W
r	Layer thickness (m)
S	Sum of squares
T	Temperature (K)
T_0	Initial temperature (K)
T_{ext}	External temperature (K)
t	Time (s)
U	Inverse of covariance matrix of parameters

\mathbf{u}	Velocity tensor (m/s)
W	Inverse of covariance of matrix of errors
X	Sensitivity matrix
X'	Scaled sensitivity coefficient
X^T	Transpose of sensitivity matrix
x_f	Thickness of fouling layer (m)
Y	Observation vector
\hat{Y}	Predicted vector of observations
<i>Greek symbols</i>	
β	Parameter
Δ	Optimal delta
Δ'	Sequential delta
μ	Dynamic viscosity (Pa·s)
μ'	Prior information of parameter β
∇	Gradient vector
Φ	Diagonal matrix ($n \times n$)
ρ	Density (kg/m^3)
<i>Subscript</i>	
i	1,2,...,n
0	Initial

ABSTRACT

Fouling is a critical issue in commercial food manufacturing. Fouling can cause biofilm formation and pose a threat to the safety of food products. Early detection of fouling can lead to informed decision making about the product's safety and quality, and effective system cleaning to avoid biofilm formation. In this study, a Non-Intrusive Continuous Sensor (NICS) was designed to estimate the thermal conductivity of the product as they flow through the system at high temperatures as an indicator of fouling. Thermal properties of food products are important for product and process design and to ensure food safety. Online monitoring of thermal properties during production and development stages at higher processing temperatures, $\sim 140^{\circ}\text{C}$ like current aseptic processes, is not possible due to limitations in sensing technology and safety concerns due to high temperature and pressure conditions. Such an in-line and noninvasive sensor can provide information about fouling layer formation, food safety issues, and quality degradation of the products. A computational fluid dynamics model was developed to simulate the flow within the sensor and provide predicted data output. Glycerol, water, 4% potato starch solution, reconstituted non-fat dry milk (NFDM), and heavy whipping cream (HWC) were selected as products with the latter two for fouling layer thickness studies. The product and fouling layer thermal conductivities were estimated at high temperatures ($\sim 140^{\circ}\text{C}$). Scaled sensitivity coefficients and optimal experimental design were taken into consideration to improve the accuracy of parameter estimates. Glycerol, water, 4% potato starch, NFDM, and HWC were estimated to have thermal conductivities of 0.292 ± 0.006 , 0.638 ± 0.013 , 0.487 ± 0.009 , 0.598 ± 0.010 , and 0.359 ± 0.008 W/(m·K), respectively. The thermal conductivity of the fouling layer decreased as the processing time increased. At the end of one hour process time, thermal conductivity achieved an average minimum of 0.365 ± 0.079 W/(m·K) and 0.097 ± 0.037 W/(m·K) for NFDM and HWC fouling,

respectively. The sensor's novelty lies in the short duration of the experiments, the non-intrusive aspect of its measurements, and its implementation for commercial manufacturing.

Keywords: CFD modeling, Fouling, Optimal experimental design, Parameter estimation, Thermal conductivity.

CHAPTER 1. INTRODUCTION

Fouling is defined as the unwanted accumulation of solids on a surface (Awad, 2011; Bott, 1995; Ibrahim, 2012; Schlüter et al., 2019). In food processing the most dramatic cases of fouling are typically observed in the dairy industry with the formation of β -lactoglobulin or calcium carbonate (CaCO_3) deposits after milk pasteurization. When dairy products are exposed to high temperatures, proteins unfold, aggregate, and start to deposit to the surface of the system (Caruyer et al., 2016). As time progresses, the deposit grows reducing the cross-sectional diameter of the system and flow rate, pressure, and thermal resistance all increase (Ibrahim, 2012). This leads to an increase in the heating provided to compensate for the extra resistance to ensure the product still receives the same thermal treatment, so it is still safe for consumption. An increase in the heating profile means higher utility usage, higher power consumption, and, therefore, an increased fuel usage causing an environmental impact (Gudmundsson et al., 2016). About 80% of dairy industry total production costs due to fouling and cleaning of process equipment (Bansal & Chen, 2006). Recent studies in processing technologies have reported Cleaning in Place (CIP) times of around 4 to 6 hours per day for the dairy industry due to fouling (Gillham et al., 1999). This leads to extra maintenance and prevention costs such as over-dimensioned equipment to compensate for the deposit formation and more frequent cleaning (Ibrahim, 2012).

With more application of technology and rigorous food safety regulations today, the food industry finds itself in need of monitoring its products in-line with specifications as much as possible. Automated systems such as visual inspections have gained popularity due to the increasing demand and speed of production. In-situ microscopy devices such as the particle vision microscope, particle image analyzer, and Envirocam have been developed to monitor

crystallization processes, characterization of particles, and general corrosion observation (Bluma et al., 2010). A variety of inline sensors have been developed in order to fine-tune food processes. These tend to monitor variables such as pressure, viscosity, flow, and most commonly temperature (McFarlane, 1995). Pinder & Gatley (1993) described several flow cytometry variations that are used to detect different microbial characteristics of food products in a system, some require previous preparations to be made. These are mostly employed to detect unwanted materials inside a food matrix and can range from color cameras to X-rays and ultrasound (Chan & Batchelor, 1993).

The design of thermal processes requires important thermal properties such as thermal conductivity, specific heat capacity and microbial inactivation parameters (D and z values). These properties are valuable to develop mathematical models to predict the temperature profile, microbial lethality and heating time. These properties are temperature dependent and have commonly been studied separately from the production lines. Common transient methods for determining thermal conductivity include the pulsed power technique, 3ω method, transient plate source for solids, the transient hot wire for fluids and solids, and the laser flash diffusivity (Zhao et al., 2016).

Many researchers have preferred the transient hot wire method because of its ease of manufacturing and use. Few instruments have been designed to accurately measure these properties at high temperatures (>100 °C). Thermal conductivity of low porosity food powders was measured by the thermal conductivity probe method as a function of porosity, moisture content, and temperature (Shah et al., 2000). Gratzek and Toledo (1993) measured the thermal conductivity of solid carrots and potatoes using a line heat source probe adapted to work at 130 °C and demonstrated how thermal conductivity decreases in more porous matrices but is on the other hand

increased with higher moisture content. In another study, an instrument named “TPCell” consisting of a small sample holder and incorporated heater was developed to estimate temperature dependent thermal properties of liquid and solid products up to 140 °C; several products were tested and their thermal conductivities were reported (Mishra et al., 2016). Wang and Hayakawa (1993) used a line heat source probe method and a specially designed sample holder to determine the thermal conductivities of starch gels at 80 to 120 °C.

Lack of accuracy (especially at elevated temperatures) and feasibility of online implementation of current sensors and probes has led to the use of inverse method approach to estimate thermal parameters of food. Inverse method uses minimization of sum of squares between the dependent variable of the numerical method and experimental data obtained through different methods. An iterative scheme was implemented as a sequential estimation procedure to provide an accurate estimate of the parameter (e.g. thermal conductivity) considering all experimental and computational errors. A study estimated the apparent thermal conductivity of carrot puree during freezing by recording the known core temperature with a probe thermocouple and applying the differential evolution method (Mariani et al., 2009). Monteau (2008) estimated the variation in thermal conductivity of sandwich bread due to changes in temperature and local water content using a temperature probe at the center of the sample. In that study, they concluded that the value of specific heat had to be precise; otherwise, the estimate of thermal conductivity would have too large of an error. In another study, data collected from a thermocouple probe at the center of a steel can and the inverse method were used to estimate the thermal conductivity of cherry pomace during non-isothermal heating (Greiby et al., 2014).

To the best of our knowledge, there are no studies available in literature where thermal properties were measured in a continuous flow system. In this study, a Non-Intrusive Continuous

Sensor (NICS) was designed to determine the thermal conductivity of a fouling layer by first calibrating against varying products in-line to provide better insight into the design of an optimal process. By using surface temperature measurements and combining it with the inverse method of estimation, NICS can provide an estimated thermal conductivity considering the effect of flow on the products' properties. This sensor could be used in future applications to determine fouling deposition and resuspension rates and thickness of a forming fouling layer without the need to dismantle the system.

CHAPTER 2. LITERATURE REVIEW

2.1 Aseptic Processing of Foods

An aseptic process is the commercial sterilization of a food or beverage in a system that has been sterilized beforehand and is maintained sterile during processing and then filled into pre-sterilized packaging (David et al., 2012; FSIS, 2014). The aseptic processing of foods came as a response to the impact of thermal processing and re-contamination on the final product quality. The idea behind aseptic processing is to eliminate any possibility of product contamination at any point during its processing and packaging. Therefore, these systems are based on continuous flow operations starting from the mixing and formulation, generally going through thermal processing, and finalizing in filling and packaging. Ultra-high temperature (UHT) sterilization systems have adopted the sterile packagers and fillers so are now considered aseptic processes. Some typical processing times for different products have been adapted from Lewis (2000) and are shown in Table 2.1. Typical UHT sterilization processes.

Table 2.1. Typical UHT sterilization processes.

Fluid food product	Temperature (°C)	Time (s)
Acid foods, pH < 4.5	93-96	15 – 30
Low-acid foods, pH > 4.5	135-149	1 – 30
Milk (USA)	138	2
Milk (UK)	> 135	> 1
Flavored milks (UK)	> 140	> 2

Source: Lewis (2000)

The thermal treatment in a retort process is more severe than in an aseptic process since it holds temperature of 121 °C for low-acid and 100 °C for high acid foods for times ranging from 15 – 45 minutes (Saravacos & Kostaropoulos, 2016). Retorts sterilize the product once inside the

container, which has a hermetic seal that prevents the product from re-contamination. The basic retort process starts by loading the system with the product in its containers then closing the vessel and turning the steam on and venting all trapped air. During the holding period, condensed steam exits through the bottom. Even though the required temperatures for sterilization are achieved with a 0.5 °C range, there is no control of the internal gradient heating of the product (May NS, 2001).

The advantage of aseptic processing compared to in-pack processing such as retorts lies in the fact that higher processing temperatures for a shorter time are possible because the product is sterilized before it is packed into pre-sterilized containers in a sterile atmosphere (Fellows 2000). In general, shorter holding times at higher treatment temperatures promote an improved product quality, while the same safety level can be maintained (Richardson 2010).

2.2 Fouling

2.2.1 Types of Fouling

Traditional methods to detect fouling require either expensive equipment or great effort in dismantling the aseptic system and prolonged shut-down times for this practice. Wallhäüßer et al. (2012) have identified several types of fouling: precipitation, particulate/sedimentation, corrosion, chemical reaction, solidification, and biofilm. Precipitation happens with the crystallization of salts and oxides. An example of this type is dairy fouling type B, especially when calcium deposits form (Figure 2.1). Particulate/sedimentation occurs when particles accumulate on surfaces such as colloids or dust. Corrosion is specific to deposits on metal surfaces such as rust. Chemical reaction refers to the decomposition of proteins and carbohydrates on heat transfer surfaces. An example of this is dairy fouling type A when protein from the milk deposits due to denaturation (Figure 2.1). Solidification refers to accumulated frozen material on a cool surface. Biofilm refers to the

growth of fungi and/or bacteria on a surface; this is especially noticeable in membrane separation systems (Wallhäußer et al., 2012).

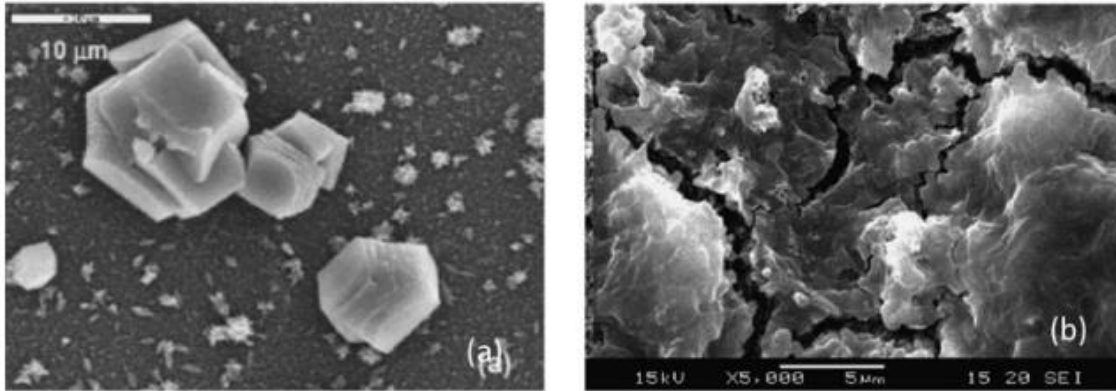


Figure 2.1. SEM imaging of fouling. (a) Type B fouling, CaCO₃ deposits. (b) Type A fouling, protein, and carbohydrate complex. Figure from (Thamaraiselvan & Noel, 2015)

2.2.2 Methods for Fouling Detection

Wallhäußer et al., (2012) compared several detection methods based on the advantages and limitations of each (Table 2.2). Heat transfer parameters and temperature detection methods lack sensitivity and are unstable at high temperatures.

Table 2.2. Comparison of different detection methods together with their advantages and limitations.

Methods	Short Description	Advantages	Limitations
Pressure drop	Pressure between inlet and outlet measured	No extra equipment Usually measured Caution of excessive pressures	Not very sensitive More sensitive for PHE Fouling place unknown
Temperature	Product outlet/heating medium temperature measured	No extra equipment Usually measured	Not very sensitive Thin layers not monitored Fouling place unknown
Heat transfer parameters	Heat flux, heat transfer coefficient,	No extra equipment (despite heat flux)	Certain thickness necessary

	thermal resistance measured	Flow/temperature usually measured	Heat flux sensors not usable at high temperatures
Electrical parameters	Electrical resistance, conductivity measured Electrical behavior of heater monitored	Very sensitive to thin layers Fouling thickness determinable	Invasive Electrical heating not popular
Acoustic/Ultrasound/QCM/QCM-D	Acoustic parameters measured Frequency change and energy dissipation monitored	Non-invasive Very sensitive to material changes, thin fouling Fouling and cleaning monitored Movable clamp-on sensor	Scattering can occur Parameters temperature dependent One transducer: only one point monitored QCM/QCM-D invasive
Numerical methods/ANN	Clean/fouled heat exchangers modelled Parameters combined in ANN	No extra equipment Very sensitive when appropriate parameters and models used	Due to parameters errors may occur First, validation with other methods necessary

Source: Wallhäußer et al., (2012)

Crattelet et al. (2013) put together a very comprehensive table of the industrial and laboratory techniques to monitor fouling (Table 2.3). Despite the many innovative methods presented, most of them either require extensive instrumentation, transparent equipment, or are lab-scale and not applicable to industrial levels.

Table 2.3. Classification of techniques to monitor fouling or product changes – Scientific or Industrial application (Sc/Ind), batch or continuous process (B/C), local or global measurements (L/G), intrusive or non-intrusive sensors (In/N-In), On-line or Post-Process (OL/PP) and Direct or Indirect thickness estimation (D/Ind).

Methods/sensors	Level	Process	L/G	In/N-In	OL/PP	Di/Ind
<i>Mechanical method</i>						
Pressure drop	Ind.	C	G	N-In	OL	Ind
Deposit weight	Sc.	C	G	In	PP	Di

<i>Thermal methods</i>						
Temperature gauge	Ind.	C	G	In	OL	Ind
Heat flux sensor	Sc.	B/C	L	N-In	OL	Ind
Hot wire method	Sc.	B/C	L	In	OL	Ind
Differential thermal analyse	Ind.	C	L	In	OL	Ind
 <i>Ultrasonic/acoustic method</i>						
Ultrasonic frequency domain reflectometry	Sc.	C	L	N-In	OL	Ind
Piezo-electric crystal	Sc.	C	L	In	OL	Ind
 <i>Electrical method</i>						
Redox potential electrodes	Ind.	B/C	L	In	OL	Ind
Electrical resistance or conductivity	Sc.	C	L	In	OL	Ind
Dielectric sensor	Sc.	C	L	In	OL	Ind
 <i>Optical Method</i>						
Turbidimeter	Sc.	B	L	N-In	OL	Ind
Spectrometry, bioluminescence, fluorometry	Sc.	B	L	N-In	OL	Ind
Optic fiber	Ind.	B	L	N-In	OL	Ind

Source: Crattelet et al. (2013)

The inexpensive thermal methods such as the heat flux sensor, which is the most similar to the presented in this research, lack accuracy compared to the expensive optical or ultrasonic methods. However, none of the sensors presented in these studies use thermal conductivity as an indicator. None of the measurements are being processed with sequential parameter estimation. This leads to unreported deviations and no discussion regarding the errors of said measurements.

2.3 Thermal Properties of Foods

Food matrices are complex systems which properties vary greatly depending on its composition. When exposed to oxygen, moisture, and temperature or a combination of these, the characteristics of a food matrix will change over time. Thermal properties like specific heat

capacity or thermal conductivity and diffusivity are also affected by composition and external factors and are important properties to study to design an appropriate process for each product. Choi & Okos (1986) developed several models to predict the thermal properties of the most common components of foods (i.e. water, protein, fat, carbohydrate, fiber, and ash) as a function of temperature (Table 2.4).

Table 2.4. Thermal property models for food components ($-40 \leq t \leq 300$ °F)

Thermal Property	Component	Thermal Property Model
Thermal Conductivity, Btu/h•ft•°F	Water	$k = 3.1064 \times 10^{-1} + 6.4226 \times 10^{-4}t - 1.1955 \times 10^{-6}t^2$
	Protein	$k = 9.0535 \times 10^{-2} + 4.1486 \times 10^{-4}t - 4.8467 \times 10^{-7}t^2$
	Fat	$k = 1.0722 \times 10^{-1} - 8.6581 \times 10^{-5}t - 3.1652 \times 10^{-8}t^2$
	Carbohydrate	$k = 1.0133 \times 10^{-1} + 4.9478 \times 10^{-4}t - 7.7238 \times 10^{-7}t^2$
	Fiber	$k = 9.2499 \times 10^{-2} + 4.3731 \times 10^{-4}t - 5.6500 \times 10^{-7}t^2$
	Ash	$k = 1.7553 \times 10^{-1} + 4.8292 \times 10^{-4}t - 5.1839 \times 10^{-7}t^2$
Specific Heat, Btu/lb•°F	Water	$c_p = 9.9827 \times 10^{-1} - 3.7879 \times 10^{-5}t + 4.0347 \times 10^{-7}t^2$
	Protein	$c_p = 4.7442 \times 10^{-1} + 1.6661 \times 10^{-4}t - 9.6784 \times 10^{-8}t^2$
	Fat	$c_p = 4.6730 \times 10^{-1} + 2.1815 \times 10^{-4}t - 3.5391 \times 10^{-7}t^2$
	Carbohydrate	$c_p = 3.6114 \times 10^{-1} + 2.8843 \times 10^{-4}t - 4.3788 \times 10^{-7}t^2$
	Fiber	$c_p = 4.3276 \times 10^{-1} + 2.6485 \times 10^{-4}t - 3.4285 \times 10^{-7}t^2$
	Ash	$c_p = 2.5266 \times 10^{-1} + 2.6810 \times 10^{-4}t - 2.7141 \times 10^{-7}t^2$
Density, lb/ft ³	Water	$\rho = 6.2174 \times 10^1 + 4.7425 \times 10^{-3}t - 7.2397 \times 10^{-8}t^2$
	Protein	$\rho = 8.3599 \times 10^1 - 1.7979 \times 10^{-2}t$
	Fat	$\rho = 5.8246 \times 10^1 - 1.4482 \times 10^{-2}t$
	Carbohydrate	$\rho = 1.0017 \times 10^2 - 1.0767 \times 10^{-2}t$
	Fiber	$\rho = 8.2280 \times 10^1 - 1.2690 \times 10^{-2}t$
	Ash	$\rho = 1.5162 \times 10^2 - 9.7329 \times 10^{-3}t$
Thermal Diffusivity, ft ² /h	Water	$\alpha = 4.6428 \times 10^{-3} + 1.5289 \times 10^{-5}t - 2.8730 \times 10^{-8}t^2$
	Protein	$\alpha = 2.3170 \times 10^{-3} + 1.1364 \times 10^{-5}t - 1.7516 \times 10^{-8}t^2$
	Fat	$\alpha = 3.8358 \times 10^{-3} - 2.4128 \times 10^{-7}t - 4.5790 \times 10^{-10}t^2$
	Carbohydrate	$\alpha = 2.7387 \times 10^{-3} + 1.3198 \times 10^{-5}t - 2.7769 \times 10^{-8}t^2$
	Fiber	$\alpha = 2.4818 \times 10^{-3} + 1.2873 \times 10^{-5}t - 2.6553 \times 10^{-8}t^2$
	Ash	$\alpha = 4.5565 \times 10^{-3} + 8.9716 \times 10^{-6}t - 1.4644 \times 10^{-8}t^2$

Source: Choi & Okos (1986)

Specific heat capacity has been defined and studied deeply by many researchers. Feidt (2017) defined it as the amount of heat to be supplied to (or taken out of) the unit mass of a system in order to increase (or decrease) its temperature by one degree in a thermodynamic process. Thermal conductivity and diffusivity take this a step further and attempt to explain the heat flux in a system in one dimension while diffusivity is referent to the heat flux in a surface area or two dimensions instead. These thermal properties are immensely important when designing food processes to ensure the food will reach the temperature to achieve the microbial inactivation required.

2.4 Parameter Estimation and Inverse Problems

Parameter estimation is defined as “a discipline that provides tools for the efficient use of data in the estimation of constants appearing in mathematical models and for aiding in modeling of phenomena” (Beck & Arnold, 1977). It is one of the categories of inverse problems, the other being function estimation. In parameter estimation, the dependence of the response variable to the independent variable, the function, is already known and only the parameters within this function need to be estimated (Zueco et al., 2004). Unlike much of the research done in Food Science, when parameter estimation is used, the errors of the parameters and the statistical assumptions are not only considered but discussed (Dolan & Mishra, 2013).

2.4.1 Scaled Sensitivity Coefficients

Parameter estimation cannot be done without calculating the sensitivity coefficients (X_{ij}). The sensitivity coefficient is considered as the first derivative of a response variable considering the independent variable (Sulaiman et al., 2012) (Beck et al., 1985). They are required to establish which parameters can be estimated and how much they are affected by measurement errors (Dolan & Mishra, 2013). Since X_{ij} is a unit-less value, a common practice is to use the Scaled sensitivity

coefficients (X_i) which are obtained by multiplying the X_{ij} by the corresponding parameter to have them represent a certain percentage of the response variable and now having its units can be easily compared. Dolan & Mishra, (2013) provided guidelines on what the behavior of the X_i should be. The X_i are expected to be large compared with the response variable and uncorrelated with each other. The larger the X_i , the greater the response and the more easily parameter β_i can be estimated. If any X_i are correlated, meaning one is a linear function of another X_j , then those parameters cannot be estimated separately because the response η to both parameters will be identical (Dolan & Mishra, 2013).

2.4.2 Sequential Estimation

Sequential estimation is an iterative process used in parameter estimation as a method to optimize the result similar to ordinary least squares (OLS). Unlike OLS, sequential estimation does not use all the data at once rather it updates the estimated parameter's value as new observations are used in the process (Dolan & Mishra, 2013). As the iterative process continues, different values for the parameter will be given and therefore the errors from each new measurement is considered. Once the estimated value for a parameter reaches a constant value, then it can be considered properly estimated and the model used for it to be adequate (Sulaiman et al., 2012). In most cases, the estimated value is presented by itself and confidence intervals are often not reported in predictive models. Therefore, the accuracy of the estimates is unknown. Nevertheless, several studies have calculated and reported 95% asymptotic confidence intervals to describe the accuracy of their estimates (Greiby et al., 2014; Muramatsu et al., 2017; Sulaiman et al., 2012).

2.4.3 Parameter Estimation in Food Science

The different methods for parameter estimation are used extensively in food science. In the food microbiology area, Jewell, (2012) tested the 1-step against the 2-step method to estimate parameters in several microbial growth models. Other studies estimated microbial inactivation parameters by using data obtained from survival curves at varying (Cattani et al., 2016; Dolan & Mishra, 2013; Peleg et al., 2003). However, use of sequential estimation itself has seen more use in food processing and engineering, specifically pertaining to thermal processing. Scheerlinck et al. (2008) used sequential estimation to obtain the thermal conductivity and volumetric heat capacity of a food analog by using the temperature readings from a hot wire probe inside the product. Thermal conductivity and volumetric heat capacity for solid foods were sequentially estimated by subjecting the products to a constant heat flux from one side and insulating it from another to understand the effect of sensor location and errors resulting from each in this type of studies (Mohamed, 2009). Mishra et al. (2016) developed a benchtop instrument to estimate thermal properties of food products heated to 140 °C.

CHAPTER 3. MATERIALS AND METHODS

3.1 Product Description and Equipment Design

Regular city water; $\geq 99.5\%$ pure Glycerol (Fisher Scientific, Pittsburg, PA, USA); powdered Starch, from potato (Sigma-Aldrich Inc., St. Louis, MO, USA) solubilized at 4% (w/w); Grade A Non Fat Dry Milk (NFDM) (Michigan Milk Producers Association, Ovid, MI, USA) reconstituted at 10% and 12% (w/w), and Kroger™ Heavy Whipping Cream were selected as the processed products in the experiments and their heat capacities and densities for simulation purposes were taken from literature (Hayes, 1987; Hu et al., 2009; Lloyd et al., 1995; Wagner & Kretzschmar, 2007).

All products were processed at a flow rate of 1 L/min and a holding time of 30 seconds in a MicroThermics® 25HV lab scale UHT/HTST unit to replicate an industrial scale processing system. Preheating was kept at 90 °C while the second heat exchanger was set so the temperature at the end of the hold tube would be 140 °C. Calibration of sensor design and estimation of thermal conductivity experiments lasted ~ 150 seconds to allow the system to equilibrate before taking the next reading.

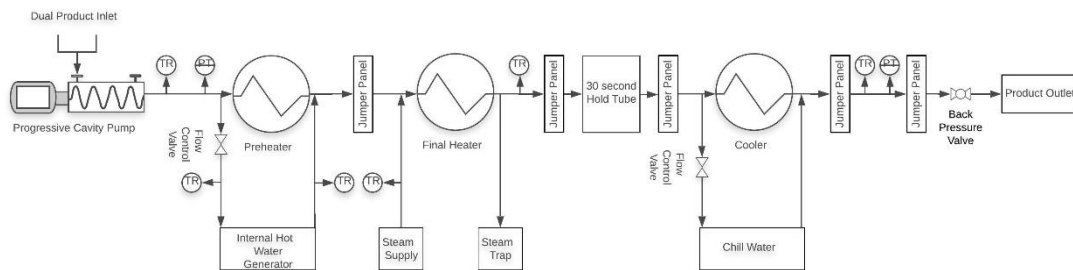


Figure 3.1. Process flow diagram for the MicroThermics 25-HV HTST/UHT lab scale unit used in study.

The non-intrusive continuous sensor (NICS) consisted of a flexible Kapton® Polyimide/FEP heater (Birk Manufacturing, Inc., East Lyme, Connecticut) and a pair of T type surface thermocouples (OMEGA, Norwalk, Connecticut) embedded underneath (Figure 3.2). The sensor was mounted on the last section of the holding tube for the sensor design and at the beginning of the holding tube for the fouling experiments.

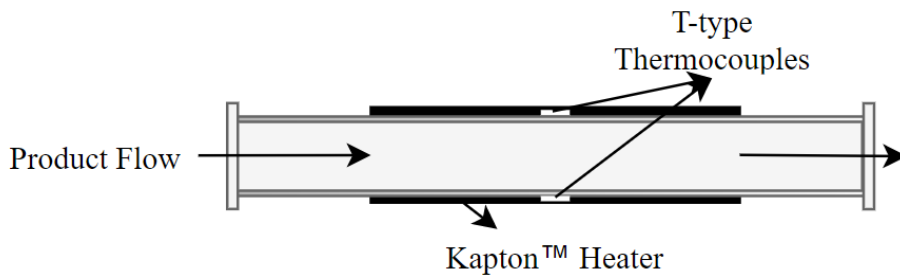


Figure 3.2. Sketch of NICS mounting on MicroThermics® unit.

3.1.1 Description of Data Acquisition

Experimental data was generated and recorded using several National Instruments™ (NI, Austin, Texas) modules. An Analog Input module (NI 9225 3-Ch. ± 300 V) measured the voltage going through the heater. A Current Input module (NI 9227 4-Ch. 5Amp) measured current and when coupled with previous module were capable of measuring power and energy consumption. A Relay module (NI 9481 4-Ch EM Form A SPST) acted as a safety switch programmed to switch off the power supply to the heater when the heater temperature was greater than 150 °C. An Analog Output Module (NI 9263 4-Ch. 100 kS/s, ± 10 V) provided specified voltage output to the heater. A Phase angle controller, FC11AL/2, (United Automation, Wheeling, Illinois) controlled the voltage coming in from power outlet to feed the voltage output module (NI 9263). A CompactDAQ chassis (cDAQ-9174 4 slot USB) also called a “bus” held the NI modules used. All thermocouples

in the system were connected to the Temperature Input Module (NI 9213 16-Ch. C Series). A Single-Module Carrier CompactDAQ Chassis (NI USB-9162) was used to carry the NI 9213 temperature module and collect its data. All the data generated and collected was controlled with National Instruments™ LabVIEW software.

3.2 Mathematical model

3.2.1 Sensor Design EQUATION CHAPTER 3 SECTION 2

A COMSOL Multiphysics® Version 5.4 model of the sensor and its mounting method on a tube was designed (Figure 3.3 and Figure 3.4). Model geometry consisted of a one-inch section of the heater, an air gap representing contact resistance, the pipe wall, and the product flowing inside a 0.381 mm internal diameter tube. Non-isothermal flow was the physics studied to numerically solve the forward problem (COMSOL, 2018). The thickness of the air gap used as contact resistance was established as the lowest possible value before COMSOL would neglect it. Maintaining it at the lowest possible value would reduce any convective effect to be negligible but would still provide a slight increase in overall heat transfer resistance to ensure model would fit experimental data more closely.

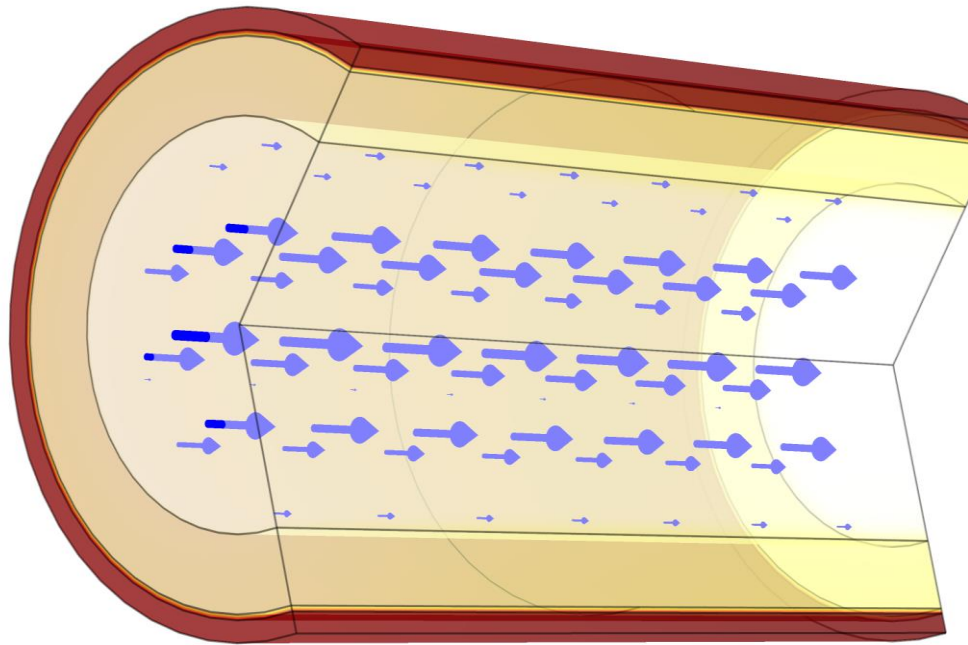


Figure 3.3. Simulated heating (red = hottest) and flow (arrow size is indicative of velocity magnitude) profile of NICS.

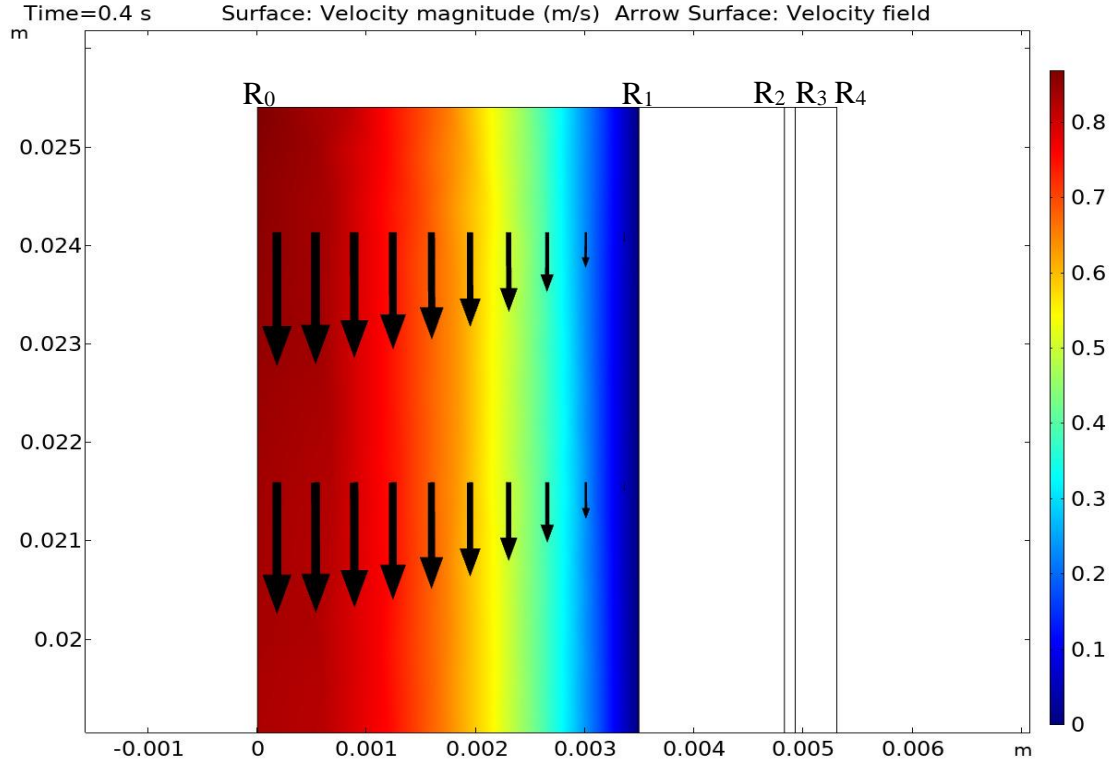


Figure 3.4. Fully developed laminar flow profile of NICS. (Arrow size is indicative of velocity magnitude)

The main governing equations for the heat transfer of solids and fluids within the system, with the heater as a heat source on the outer boundary and the product at an equilibrated temperature are:

$$\rho C \frac{\partial T}{\partial t} + \rho C \mathbf{u} \cdot \nabla T + \nabla \cdot \mathbf{q} = Q \quad [3.2.1]$$

$$\mathbf{q} = -k \nabla T \quad [3.2.2]$$

where ρ is the density of the layer, C is the specific heat of the layer, \mathbf{u} is the velocity magnitude of the layer, $\partial T / \partial t$ is the change in temperature with respect to time, ∇T is the gradient in temperature along all the geometry, \mathbf{q} is the inward heat flux, Q is the volumetric heat source, and k is the thermal conductivity of the material defined for the layer. COMSOL utilizes these general equations and solves it per every layer. In the case of the product layer flowing on the inside, $Q =$

0 and for conduction through the solid layers (i.e. pipe wall and heater) the \mathbf{u} term is zero thus disregarding any flow. Equation [3.2.1] can be broken down for each specific layer as:

$$\frac{1}{r} \frac{\partial}{\partial r} \left[k_h r \frac{\partial T}{\partial r} \right] + Q = C_h \frac{\partial T}{\partial t} \text{ for } R_3 < r \leq R_4, t > 0 \quad [3.2.3]$$

$$\frac{1}{r} \frac{\partial}{\partial r} \left[k_a r \frac{\partial T}{\partial r} \right] = C_a \frac{\partial T}{\partial t} \text{ for } R_2 < r \leq R_3, t > 0 \quad [3.2.4]$$

$$\frac{1}{r} \frac{\partial}{\partial r} \left[k_{ss} r \frac{\partial T}{\partial r} \right] = C_{ss} \frac{\partial T}{\partial t} \text{ for } R_1 < r \leq R_2, t > 0 \quad [3.2.5]$$

$$\frac{1}{r} \frac{\partial}{\partial r} \left[k_p r \frac{\partial T}{\partial r} \right] = C_p \frac{\partial T}{\partial t} + \rho C_p \mathbf{u} \cdot \nabla T \text{ for } R_0 < r \leq R_1, t > 0 \quad [3.2.6]$$

where r is the thickness of each layer and the subscripts h , a , ss , and p , represent each of the layers: heater, air, stainless steel, and product, respectively.

The initial temperature is:

$$T(r, 0) = T_0 \quad [3.2.7]$$

The boundary condition at R_4 is set to be a temperature boundary at room temperature:

$$T(R_4, t) = T_0 \quad [3.2.8]$$

The main governing equations for the laminar flow regime of the product inside the system are:

$$\rho \frac{\partial \mathbf{u}}{\partial t} + \rho(\mathbf{u} \cdot \nabla) \mathbf{u} = \nabla \cdot [-\rho \mathbf{I} + \mathbf{K}] + \mathbf{F} \quad [3.2.9]$$

$$\rho \nabla \cdot (\mathbf{u}) = 0 \quad [3.2.10]$$

$$\mathbf{K} = \mu(\nabla \mathbf{u} + (\nabla \mathbf{u})^T) \quad [3.2.11]$$

where $\partial \mathbf{u} / \partial t$ is the change in product velocity over time, \mathbf{I} is the identity matrix, \mathbf{K} is the average viscous stress tensor, \mathbf{F} is the sum of all forces acting in the system, and μ is the dynamic viscosity.

Every system requires a set of boundary conditions that need to be established. This system has a no slip wall condition between the product and the pipe wall represented by:

$$\mathbf{u} = \mathbf{0} \quad [3.2.12]$$

Fully developed flow is considered therefore,

$$\mathbf{u} \cdot \mathbf{t} = 0 \quad [3.2.13]$$

which shows how at any time point t , there will be no wall slippage or movement and equation [3.2.14] is used to define the classic parabola shaped profile in fully developed laminar flow.

$$[-\rho\mathbf{I} + \mathbf{K}]\mathbf{n} = -\rho_{grad}\mathbf{n} \quad [3.2.14]$$

Pressure boundary has been defined to suppress backflow, and is represented by

$$[-\rho\mathbf{I} + \mathbf{K}]\mathbf{n} = -\hat{\rho}_0\mathbf{n} \quad [3.2.15]$$

$$\hat{\rho}_0 \leq \rho_0 \quad [3.2.16]$$

Initial temperature (~140 °C) was defined as the inlet temperature of the product at sensor location before power was supplied to the heater to generate a heat pulse that would achieve a certain temperature in the sensor from where the k of the products would be estimated. Finally, the mesh was dependent on the physics studied and was defined as a free tetrahedral with a minimum element size of 1.5E-4 m and a maximum of 3.3E-3 m and two boundary layers between each domain.

3.2.2 Fouling layer model

The initial model was modified to include the fouling layer as shown in Figure 3.5. It was set to have a 0.5 mm thickness (from R_f to R_l) as an approximate value of the actual thickness seen in experiments. Run time for the model was increased to 60 minutes with strict intervals set at

every 5 minutes. These time steps would indicate the times at which the sensor would provide its 15 second heat pulse to stimulate the system and obtain a thermal response recorded by the thermocouples.

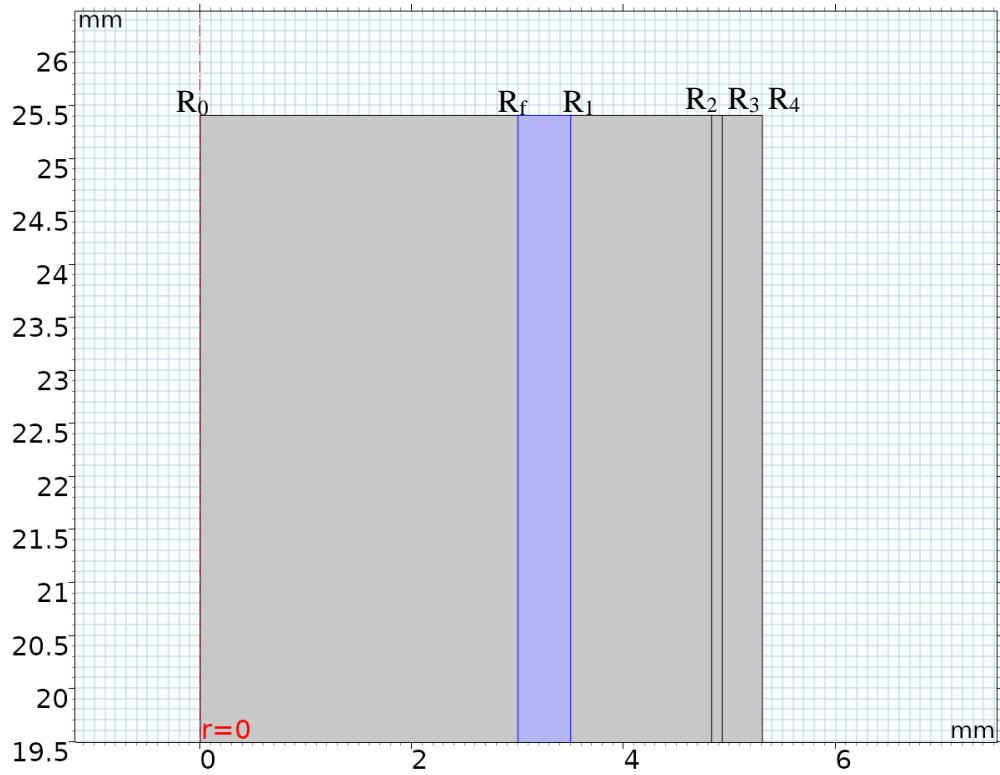


Figure 3.5. Model geometry highlighting fouling layer

The boundary condition at R_4 was modified from being a constant ambient temperature to a natural convection heat flux condition, expressed as:

$$q_0 = h(T_{ext} - T) \text{ for } R_4 \quad [3.2.17]$$

where q_0 is the boundary convective heat flux, h is the heat transfer coefficient, T_{ext} is the external temperature, and T is the temperature at the boundary. For R_4

Since a new domain has been added, the heat transfer equation for the product [3.2.6] changes to

$$\frac{1}{r} \frac{\partial}{\partial r} \left[k_p r \frac{\partial T}{\partial r} \right] = C_p \frac{\partial T}{\partial t} \rho C \mathbf{u} \cdot \nabla T \text{ for } R_0 < r \leq R_f, t > 0 \quad [3.2.18]$$

And the heat transfer equation for the added fouling layer is

$$\frac{1}{r} \frac{\partial}{\partial r} \left[k_f r \frac{\partial T}{\partial r} \right] = C_f \frac{\partial T}{\partial t} \text{ for } R_f < r \leq R_1, t > 0 \quad [3.2.19]$$

Where the subscript f stands in for fouling.

To be able to model this problem more precisely, the mesh was reduced in size in comparison to the initial model. The maximum element size for the fouling layer was set to 0.186 mm and for the rest of the model it was defined at 0.239 mm. Mesh element quality in regard to skewness was analyzed to confirm good results would be obtained (Figure 3.6). The highest value for skewness is 1 and it is based on the skew that is applied to penalize elements with larger or smaller angles than a perfect element. The average element quality in the model was 0.87 with a single element at a minimum of 0.4661.

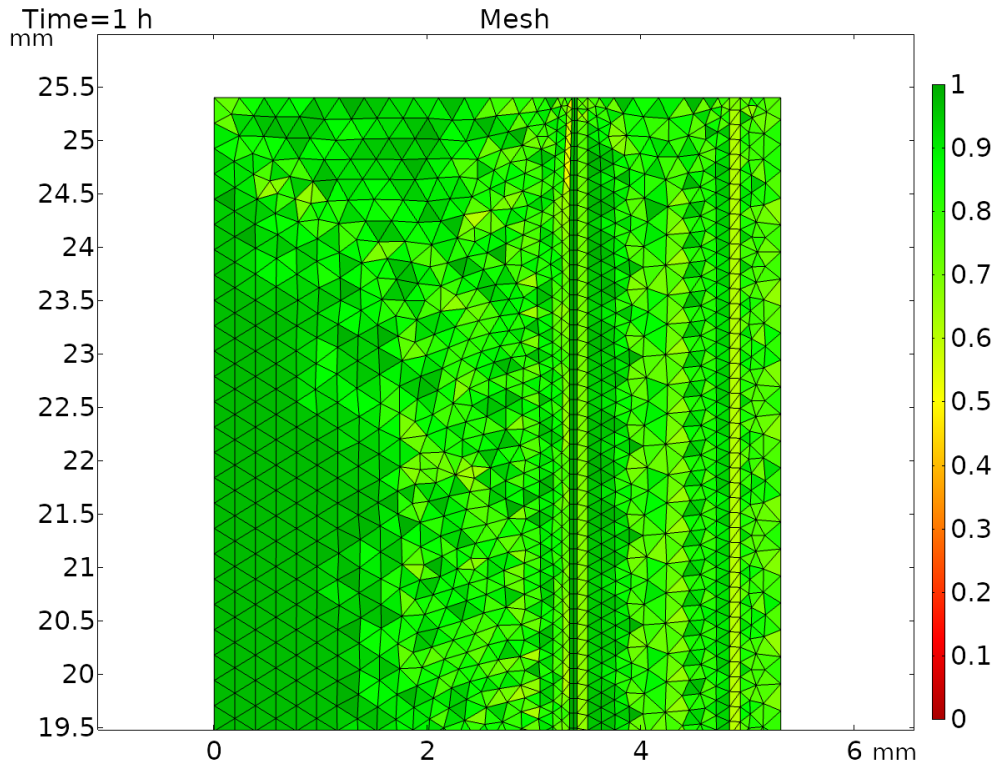


Figure 3.6. Model mesh quality (skewness) evaluation

NFDM reconstituted at 15% (w/w) and heavy whipping cream (HWC) from Kroger™ (Cincinnati, OH, USA) were selected as the fouling producing agents. All material properties used for both models are listed in Table 3.1. Material properties used in COMSOL models.

Table 3.1. Material properties used in COMSOL models.

Product/Material	Density (kg/m³)	Specific Heat (kJ/kg·K)	Thermal Conductivity (W/m·K)	Reference
Glycerol	1262	2.43	0.29	(Singh et al., 2018)
Potato starch	968	3.39	0.52	(Lloyd et al., 1995)
Water	926	4.29	0.69	(Wagner & Kretzschmar, 2007)
NFDM	1035	3.94	0.53	(Hayes, 1987; Hu et al., 2009)
HWC	1001	3.56	0.33	(Hayes, 1987; Hu et al., 2009)
316L Stainless Steel	8000	500.00	16.3	(AZO Materials, 2001)
NICS	3110	862.90	37.3	(Cardarelli, 2008)

3.3 Instrument calibration

The thermocouple probes were calibrated using a Fluke® 6109A Portable Calibration Bath. The temperature displayed by the device was recorded as the reference temperature and thermocouple readings were recorded at setpoints of 25, 50, 75, 100, 125, and 140 °C. Calibration curves were established, and a calibration coefficient was applied to the experimental data collected by the thermocouples. Power output for the heater was calibrated by selecting different voltage input settings in LabVIEW and recording the wattage. The “zero” and “span” dials on the phase angle controller were adjusted until the power output recorded at the heater was as small as possible and the power generated at different settings matched the experimental design.

The sensor calibration was done using water and glycerol as the calibrating agents as their thermal conductivities have been studied extensively, then estimation was verified on 10% NFDM and the 4% starch solution. These trials consisted of a running product through the MicroThermics unit at 140 °C while the sensor provided a ~50 W heat pulse for 15 seconds. 10 data files were obtained per trial with triplicates for a total of 60 calibration files (water and glycerol) and 60 files for the estimation of thermal conductivity of 10% NFDM and starch.

3.4 Scaled Sensitivity Coefficients **EQUATION SECTION 4**

Scaled sensitivity coefficients can be used to determine if the parameter can be estimated with low error (Dolan & Mishra, 2013). The sensitivity coefficient of a parameter is the first partial derivative of the function involving the parameter, with respect to the parameter (Beck & Arnold, 1977). The coefficient becomes scaled when it is multiplied by the parameter. The scaled sensitivity coefficient of k in this study was calculated by applying temperature gradient using equation [3.4.1]

$$X'_k = k \frac{\partial T}{\partial k} \quad [3.4.1]$$

A scaled sensitivity coefficient with a large magnitude suggests a larger model response was obtained due to changes in the parameter, in this case a larger temperature change with respect of the thermal conductivity (D'Alessandro & de Monte, 2017). If more parameters were to be estimated at the same time, their scaled sensitivity coefficients should be uncorrelated to prove that both parameters can be estimated separately (Dolan & Mishra, 2013). If the sum of the scaled sensitivity coefficients is equal to zero, then a linear dependence of the parameters exists suggesting that not all the parameters can be estimated separately (Mishra et al., 2017).

3.5 Optimal Experimental Design **EQUATION SECTION 5**

As Samsudin et al., (2018) have discussed, finding an optimal experimental design will help reduce computational time and experimental errors in the parameter estimation by ensuring that enough data has been collected. Optimal experimental design can be achieved by maximizing the determinant of the sensitivity matrix. Expressed as optimal delta

$$\Delta = |X^T X| \quad [3.5.1]$$

where X represents the sensitivity matrix and T stands in for transpose. When there are the same number of response measurements as parameters being estimated, equation [3.5.1] reduces to

$$\Delta = |X^T X| = X^2 \quad [3.5.2]$$

Thus, the optimal conditions should maximize the determinant of X (Mishra et al., 2009). Maximizing delta guarantees minimization of the confidence region. For further details on optimal experiments, readers are directed to the original work (Beck & Arnold, 1977).

3.6 Sequential Estimation EQUATION SECTION 6

After experimental data was collected, it was coupled with the COMSOL® model's (equations [3.2.1] - [3.2.17]) results via the LiveLink™ for MATLAB®. A code was developed in MATLAB® to run sequential estimation to obtain a single k value, the standard error, and a confidence interval for the product during design of the sensor. In fouling experiments, the code was modified to obtain a h for a group of observations and then estimate k for the fouling layer at every 5-minute interval based on this new heat flux and a constant k value determined for the product.

The sequential estimation procedure refers to updating the estimated parameter as new observations are added. This procedure follows the Gauss minimization method, which has been explained by Sulaiman et al., (2012) to obtain an iterative expression for the parameter to be estimated. The Gauss minimization method can be expressed as:

$$S = [Y - \hat{Y}(\beta)]^T W [Y - \hat{Y}(\beta)] + [\mu' - \beta]^T U [\mu' - \beta] \quad [3.6.1]$$

where Y is the experimental temperature matrix, \hat{Y} is the predicted temperature matrix, μ is prior information of parameter β , W is the inverse of the error covariance matrix, U is the inverse of the parameters covariance matrix, and T stands in for transpose (Mishra et al., 2016). Beck and Arnold (1977) provided an iterative sequential procedure that may be used for several types of estimations:

$$A_{i+1} = P_i X_{i+1}^T \quad [3.6.2]$$

$$\Delta'_{i+1} = \Phi_{i+1} + X_{i+1} A_{i+1} \quad [3.6.3]$$

$$K_{i+1} = A_{i+1} \Delta'_{i+1}{}^{-1} \quad [3.6.4]$$

$$e_{i+1} = Y_{i+1} - Y_{i+1} \quad [3.6.5]$$

$$b_{i+1}^* = b_i^* + K_{i+1}[e_{i+1} - X_{i+1}(b_i^* - b_i)] \quad [3.6.6]$$

This method has been used especially for in-line applications because of its capability of updating the parameter estimate as new data is collected. Readers are encouraged to refer to the original work for a more detailed explanation on the procedure (Beck & Arnold, 1977).

The 95% asymptotic confidence intervals for the estimated thermal conductivity was computed using the command in MATLAB `nlparci`.

CHAPTER 4. RESULTS AND DISCUSSION

4.1 Instrument Calibration

Data collected by each thermocouple were corrected by applying the calibration equations to them before being used in sequential estimation. Thermocouples were calibrated with an uncertainty of ± 0.0683 °C. The power calibration curve (Figure 4.1) was established to determine the proper voltage input setting to use so the heater would get enough power to see an actual temperature difference on the readings. Because of the heater's capacity, experiments were limited to a pulse of 4.6 voltage input setting providing 58 W of power for 15 seconds.

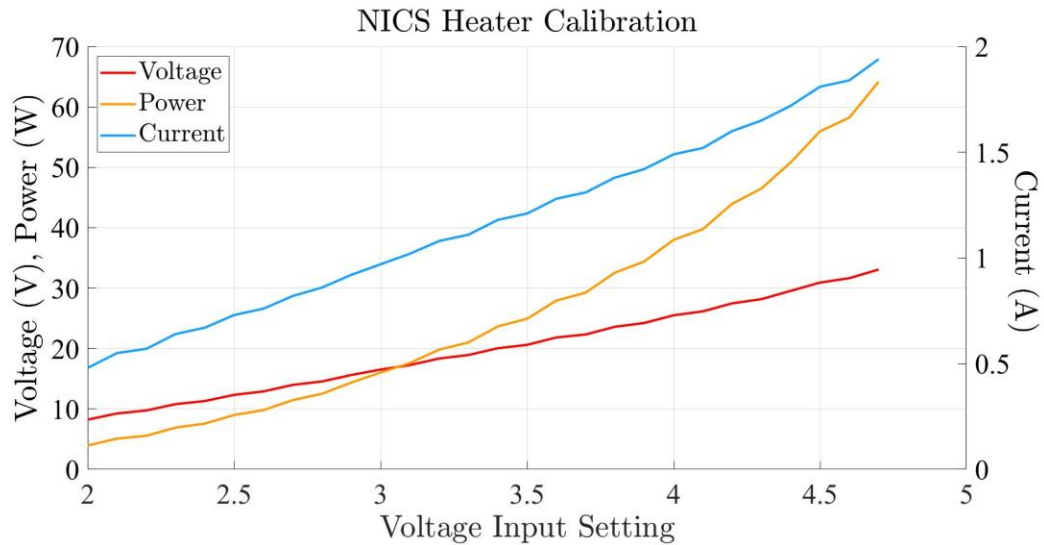


Figure 4.1. Voltage input and power calibration curve for NICS heater.

4.2 Scaled Sensitivity Coefficients

The scaled sensitivity coefficient is used to determine how sensitive the measured variable, temperature in this case, is to changes in the estimated parameter (Mishra et al., 2017). Figure 4.2. shows how as time keeps progressing, the measured temperature will be more dependent on the k .

The scaled sensitivity coefficient is expected to have a magnitude greater than 10% of the measured response, in this case temperature. In the Glycerol experiments at room temperature, the average increase in temperature was of 19.78°C and the average SSC was 8.98 which represents a 45.39%. This provides insight that k can be accurately estimated with small standard error. The average SSC percentages for water, 10% NFDM, and starch were 45.64, 52.56, and 44.22%, respectively.

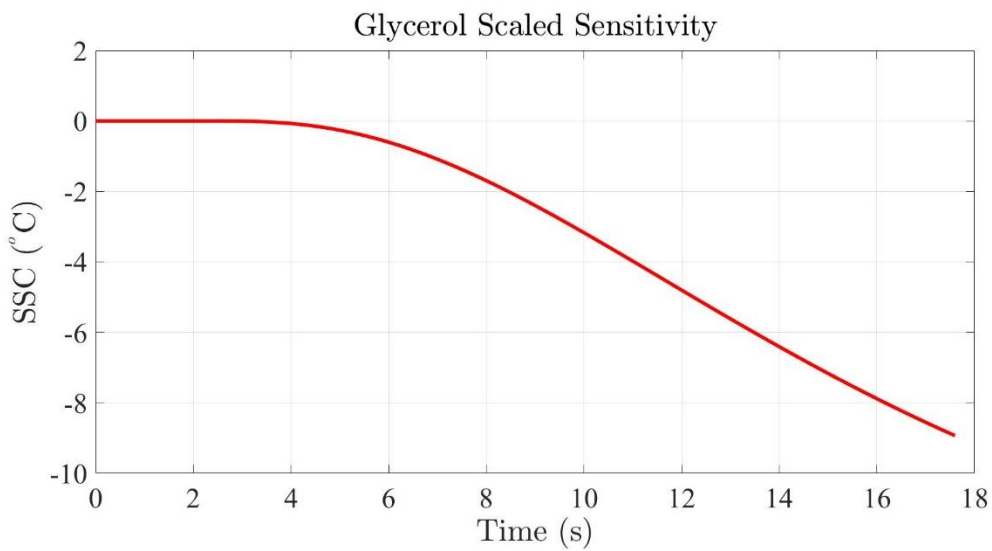


Figure 4.2. Scaled sensitivity coefficient (SSC) for estimation of the thermal conductivity of Glycerol at room temperature.

If duration of pulse were less than 6 seconds, k would not be estimated properly. Preliminary experiments with pulses of shorter duration (2 s) resulted in scaled sensitivity coefficients that represented only a 12.73% of the increase in temperature. This shows how scaled sensitivity coefficients can be useful to determine data usefulness and design proper experiments.

4.3 Optimal Experimental Design

The optimal delta values obtained for the different pulse times and powers (Figure 4.3) show how a longer pulse with a higher power will reduce the errors in estimation. Nevertheless, the data logging equipment was limited to the pulse power of ~58 W. Each pulse was held for 15 seconds. These settings also ensured that the temperature rise would not be too large for the experiment.

Multiple trials for each product were monitored and their temperature profiles were plotted against the predicted data from the model. Figure 4.4. shows the change in temperature generated by the sensor's heat pulse from one of the trials done on 10% NFDm.

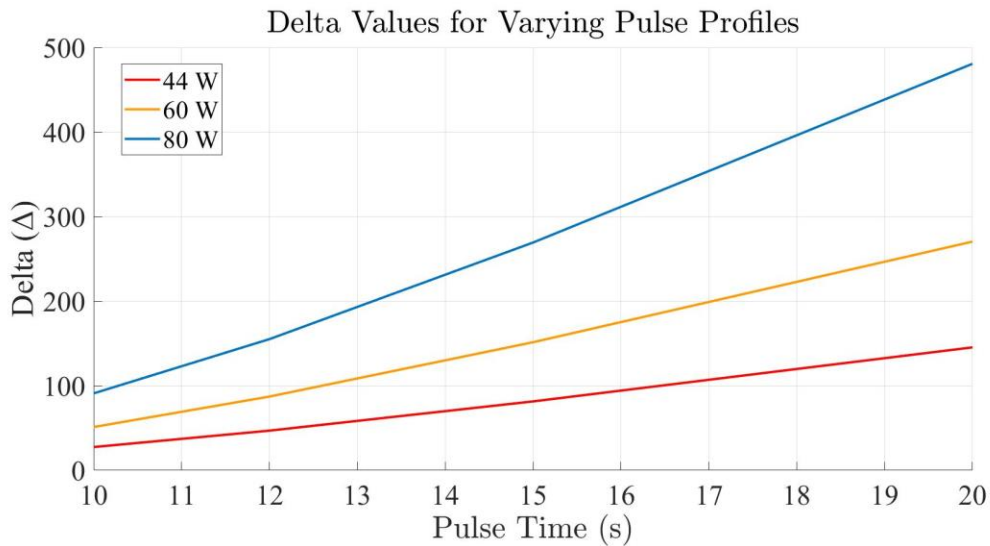


Figure 4.3. Delta values obtained for different time-power (pulse) profiles for heater in NICS.

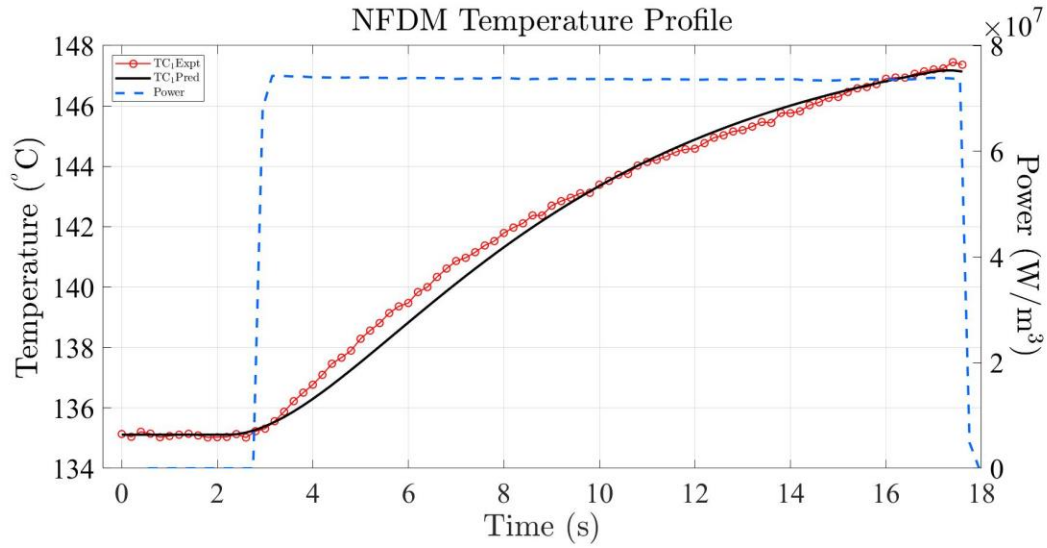


Figure 4.4. Temperature profile of a 10% NFDM trial showing the heat generated by the sensor.

A slight pattern can be detected in the residuals plot (Figure 4.5) resulting from the discrepancies between the model's predicted data and the experimental data. Many possible reasons for this difference exist. One reason might be the contact resistance of the inner layers of the heater and therefore the experimental temperature is slightly different from the model temperature, especially at early times. Another explanation is the lack of information of the heater thermal properties supplied by the manufacturer leading to researcher to calculate them based on literature values for each layer of material within the heater. We expect that with better thin film heater and actual values of heater properties would improve the residuals. However, it is expected to have some correlation in residuals for continuous data acquisitions (Beck & Arnold, 1977).

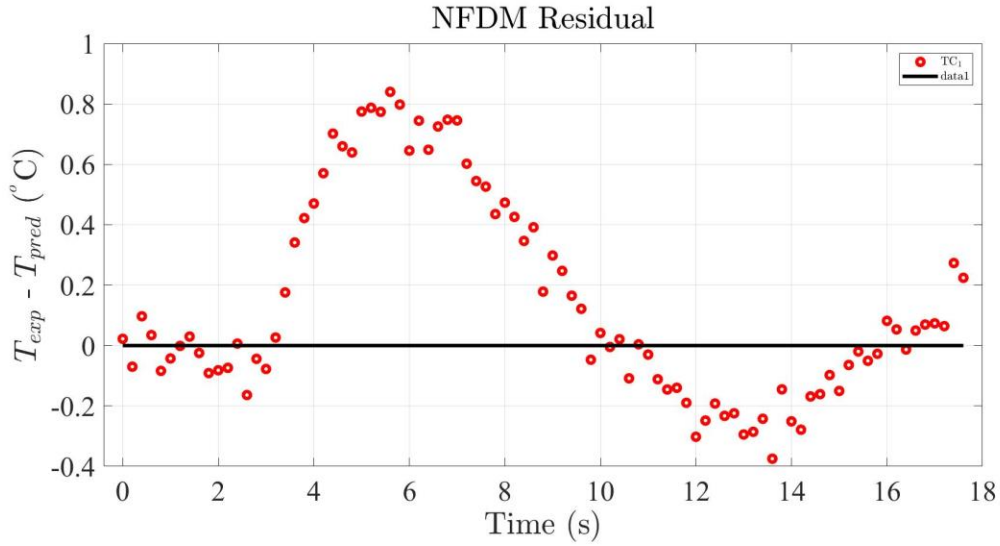


Figure 4.5. Residual plot for a 10% NFDM trial showing difference between experimental and predicted data.

The general behavior for the rest of the products selected in this study follows a similar pattern and is therefore not shown.

4.4 Sequential Estimation of Thermal Conductivity

4.4.1 Sensor Calibration

Sequential estimation updates the parameter estimate as new data points are being added but is expected to reach a constant value considered to be the real thermal conductivity (Sulaiman et al., 2012). Initial guesses for the thermal conductivity of glycerol, starch, 10% NFDM, and water were 0.3, 0.5, 0.5, and 0.6, respectively. As shown in Figure 4.6., the estimated k for glycerol reaches a steady value of 0.29 ± 0.0064 W/(m·K).

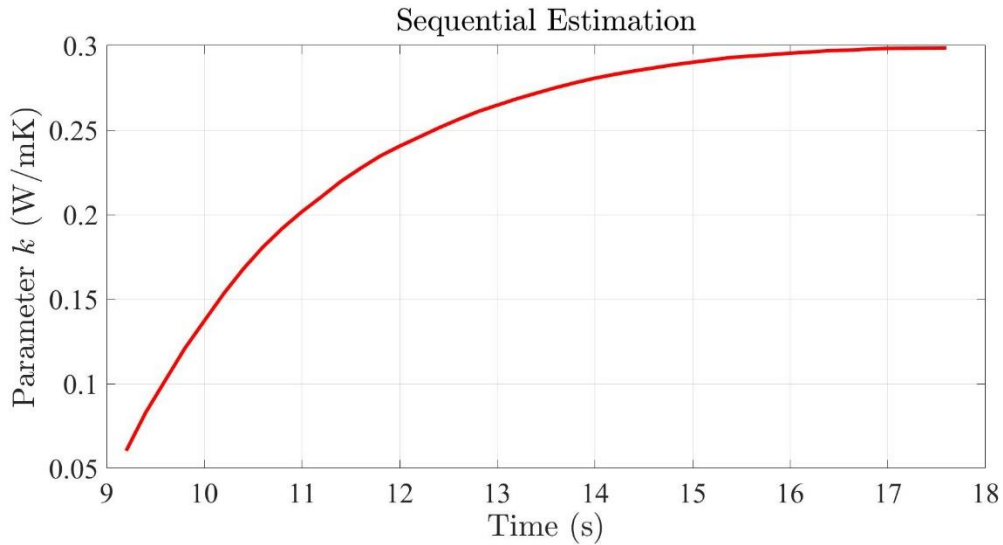


Figure 4.6. Thermal conductivity of Glycerol updated at every new data point.

Sequential estimation plots for starch, water, and 10% NFDM have a similar overall behavior and are therefore not shown.

The box-and-whiskers plot presented in Figure 4.7 is a great way to represent the variability and precision of the estimated values for the different products by providing a quantitative measure when analyzing the interquartile range (IQR). The IQR is the range between the 25th and the 75th quartile, represents 50% of the data collected, and is useful to identify outliers and their severity. A lower IQR represents a smaller variation between results, the lowest here is presented by glycerol at 0.009 W/(m·K). The highest IQR was in the potato starch with a value of 0.06 W/(m·K) followed by 10% NFDM and water at 0.04 and 0.03 W/(m·K), respectively. Values that lie above $Q3 + 1.5IQR$ or below $Q1 - 1.5IQR$ are outliers. These are only found in 10% NFDM results and can be a result of fouling in the system. Further research on sensor application to fouling are required to study the impact of fouling on estimated thermal conductivity. We could confirm, visually the existence of a fouling layer in tube after the trials with 10% NFDM.

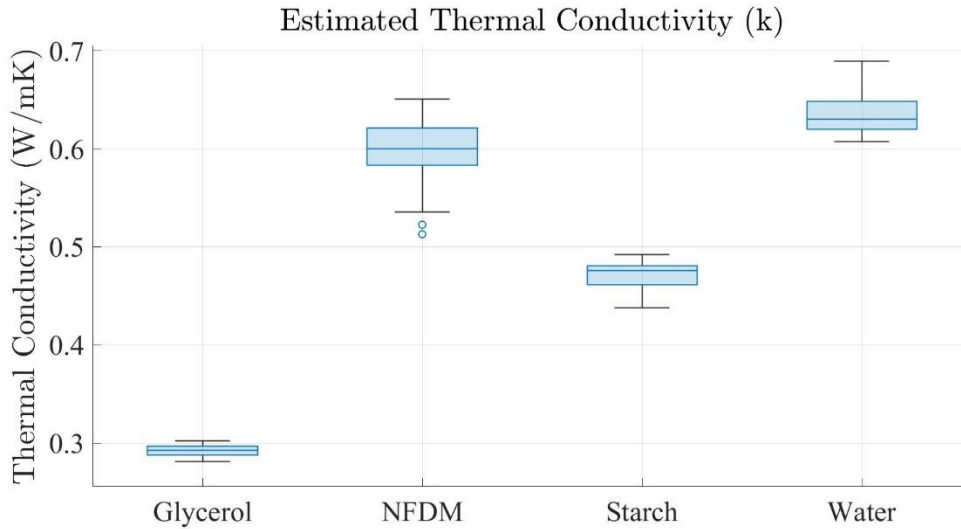


Figure 4.7. Box-and-whisker plot showing the variability of the estimated thermal conductivities for the products used in the study.

The mean estimated thermal conductivity for starch, NFDM, water, and glycerol and their corresponding mean standard deviations along with their 95% confidence intervals are shown in Table 4.1.

Table 4.1. Mean estimated thermal conductivities for all products and their corresponding 95% confidence interval (CI)

Product	Mean Thermal Conductivity (W/(m·K))	Std. error	Lower CI	Upper CI
Glycerol	0.2919	0.0064	0.2887	0.2952
Water	0.6384	0.0125	0.6329	0.6439
4% Starch	0.4873	0.0086	0.4835	0.4911
10% NFDM	0.5977	0.0104	0.5934	0.6020

Glycerol is considered the standard since its thermal properties have been studied for a long time and its k does not vary greatly with temperature as most food products do (Singh et al., 2018). The estimated values are in accordance with those found by Verma, Singh, & Chaudhary (1993) who obtained thermal conductivity values for glycerol of 0.292, 0.297, and 0.270 W/(m·K)

with varying methods at room temperature (20 °C). Thermal conductivity values of 0.2855 ± 0.0019 W/(m·K) have been reported as well (Gustafsson et al., 1979).

Thermal properties of water have been studied greatly and most of the literature presenting them were published several years ago. The Food Engineering Data Handbook listed the thermal conductivity of water to be 0.684 W/(m·K) (Hayes, 1987). Other values for the thermal conductivity of water have been listed as 0.6723 W/(m·K) at 97 °C (Ramires et al., 1995), 0.67 – 0.69 W/(m·K) between 100 – 150 °C (Coker, 2007), and a maximum of 0.686 W/(m·K) at 137 °C was reported by the National Bureau of Standards (Ho et al., 1968).

The estimated values obtained for potato starch are similar to those reported by Wang & Hayakawa, (1993) who reported k at 120 °C for gelatinized potato starch gels to range 0.4826 – 0.5656 W/(m·K) when moisture content ranged 49.18 – 74.97%. Buhri and Singh, (1993) designed an attachment probe for a DSC to measure thermal conductivities of foods and found potato to have a k of 0.552 ± 0.012 W/(m·K). Rice, Selman, & Abdul-Rezzak, (2007) reported thermal conductivities of whole potatoes at varying temperatures (40 – 90 °C) to be 0.41 – 0.56 W/(m·K). These results are not unlike those presented by Hayes (1987) in the Food Engineering Data Handbook who listed the thermal conductivity of whole potato to range from as low as 0.42 to 1.1 W/(m·K). Potatoes have a wide range of thermal conductivity because of the differences in composition, especially water content.

10% NFDM values obtained in this study compares to those presented in Pereira, De Resende, De Oliveira Giarola, Pinto, & De Abreu, (2013) who studied the thermal conductivity of milk with varying fat compositions. They reported values for 1% fat milk to be up to 0.63 W/(m·K) at 80 °C which compares well with the Choi and Okos, (1986) models for a thermal conductivity value of

0.64 W/(m·K) for liquid foods. This is expected since most of the composition was water and it has a reduced fat content which is the component with the lowest conductivity within the matrix.

4.4.2 Fouling Layer Thermal Conductivity Estimation

Data at every 5 minutes in a 1-hour long trial was used for every replicate of 15% NFDM and HWC to estimate the thermal conductivity of the fouling layer as time progressed. However, the system would take ~10 minutes to stabilize entirely once the transition from water to product was made and recirculation had started. Data for both products had a normal distribution except for one of the 15% NFDM trials where which had a non-normal distribution and had a significantly different mean from the others because of this. Welch's t-test was used to understand the difference between mean and proved that all means were equal for the HWC and not all means were equal for the 15% NFDM trials.

All experiments for each trial were visualized in the same plot and normalized to view the increase in temperature caused by the sensor (Figure 4.8) to check for any trends in behavior. As the trial progressed, the increase in temperature caused by the sensor is increasing. This is expected as the formation of a fouling layer would have a lower thermal conductivity than that of the product and therefore less heat from the sensor would penetrate. To account for any discrepancies between the model's convective heat flux (h) and the experimental, different h values were estimated depending on the proximity of one data point to another. For this, intervals were made where each would have an estimated h used for the estimation of k in those time points. A clear distinction was made between the experiments from 15 to 35 minutes and those from 40 to 60 minutes. These two sections had their own h estimated and were 546.92 ± 6.19 and 557.98 ± 5.60 W/m²K. For 15% NFDM trials, the h would reach values of 194.73 ± 3.32 and 230.68 ± 2.70 W/m²K. This is to be expected due to the difference in the thermal conductivities for both products.

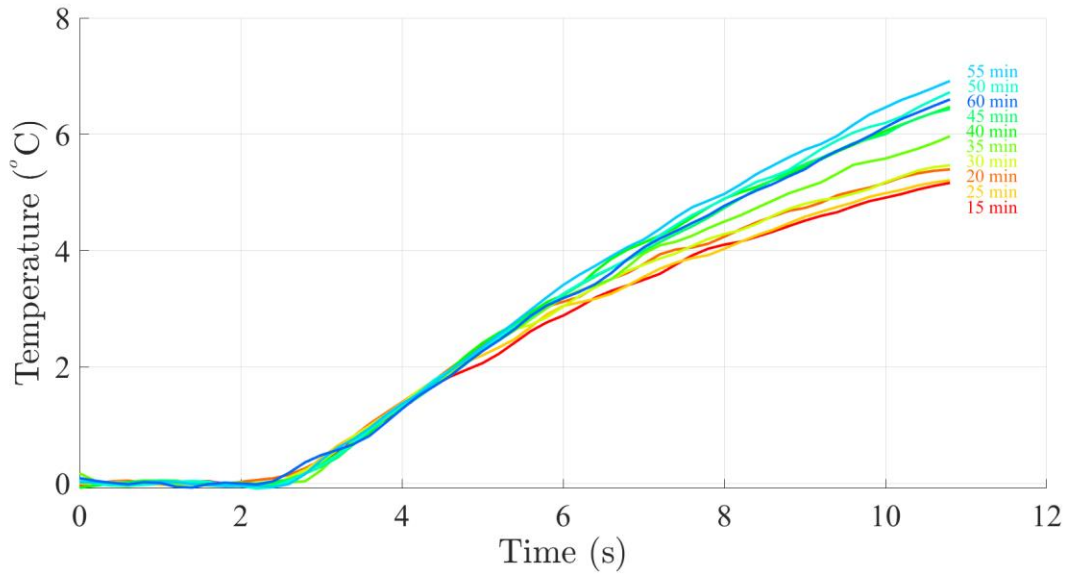


Figure 4.8. All experiments for one HWC trial plotted on a same scale to locate variances and estimate h accordingly.

Thermal conductivity was estimated for each 5-minute file once h values had been estimated for each section of the trials for each product. As with the sensor calibration, scaled sensitivity coefficients were revised to determine whether the thermal conductivity would be properly estimated at that time point. Figure 4.9 shows the scaled sensitivity coefficient of the estimation process for the HWC data collected at 45 minutes of processing. The model increase in temperature was 6.23 and the SSC reached a maximum magnitude of 0.65 meaning it represents a 10.5% of the change in temperature. As mentioned in a previous section, since it is above 10%, the thermal conductivity can be properly estimated using this model and response variable.

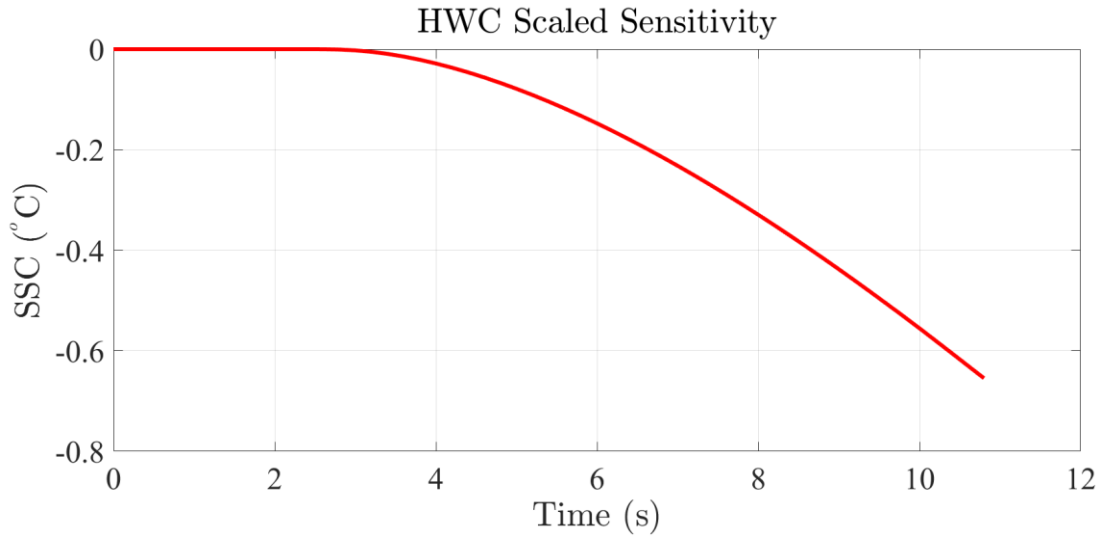


Figure 4.9. Scaled sensitivity coefficient (SSC) for estimation of the thermal conductivity of HWC at 140 °C.

Compared to the scaled sensitivity coefficients presented during the sensor calibration, these are smaller in magnitude and might imply less sensitivity of the estimated parameter (thermal conductivity of fouling layer) to changes in the measured temperature. A downward trend can be observed in the percentage of the change in temperature these coefficients represent (

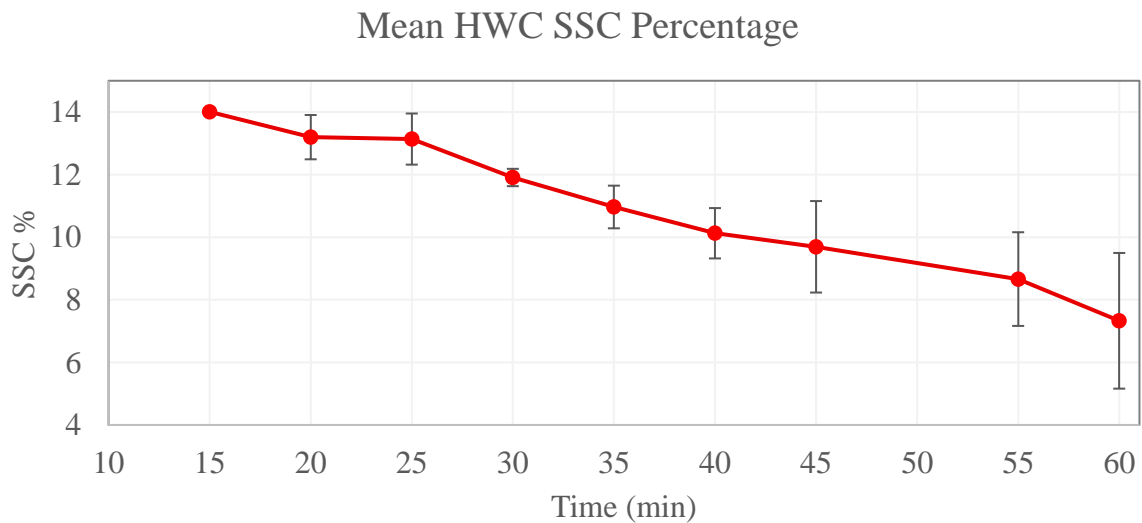


Figure 4.10 (Figure 4.11). This is very similar to that shown by the value of the thermal conductivities estimated at every 5-minute interval for each product. This could imply the sensitivity of the thermal conductivity of the fouling layer is decreasing to changes in temperature because it is becoming more and more dependent on the thickness of it instead.

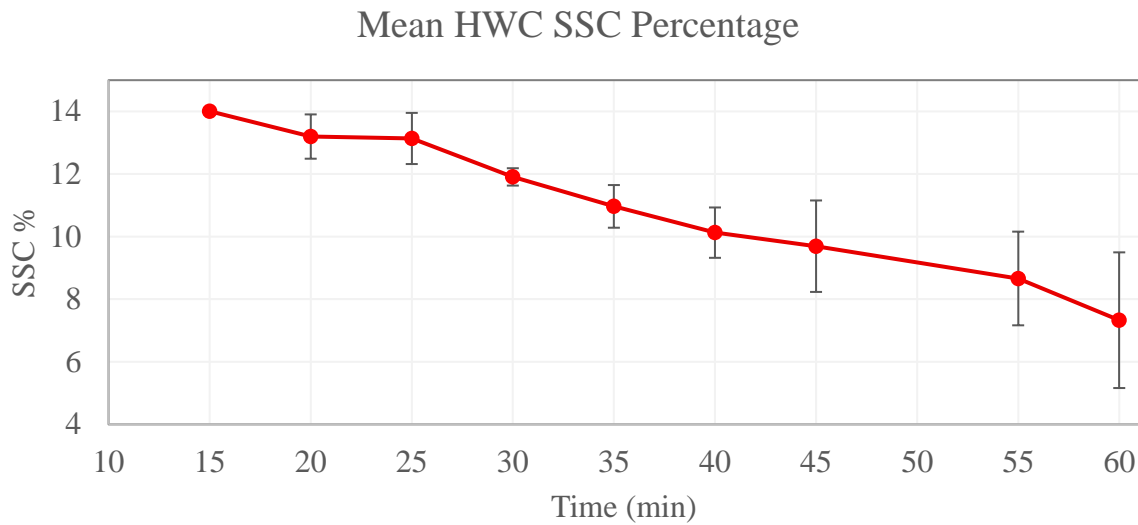


Figure 4.10. Percentage of the change in temperature represented by the SSC at each data point for HWC

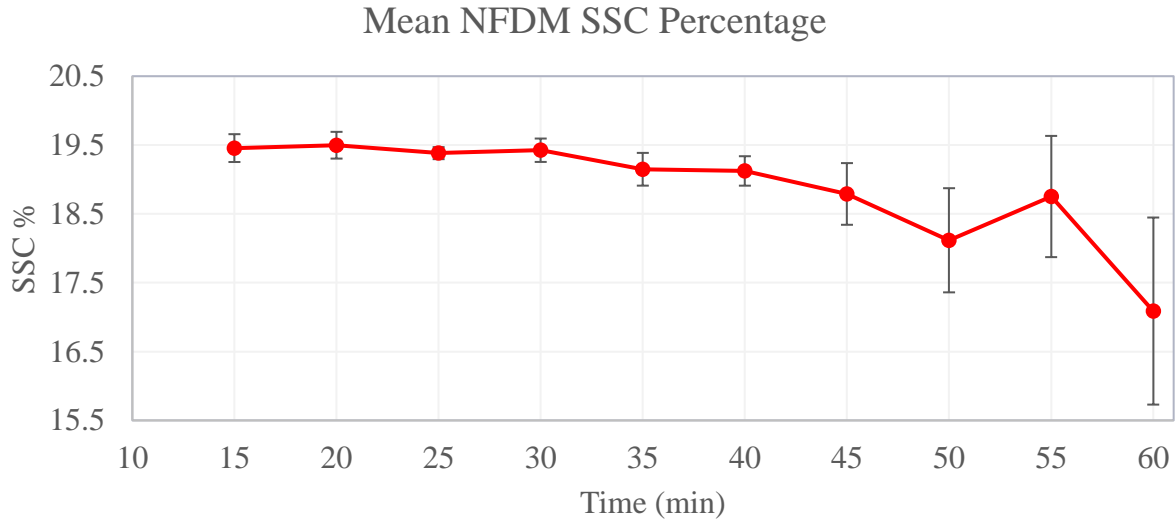


Figure 4.11. Percentage of the change in temperature represented by the SSC at each data point for NFDM.

To further understand the effect of time on the temperature recorded by the sensor, experimental and predicted data at 15 and 60 minutes of processing have been plotted to observe any differences between beginning and end of trial Figure 4.12. The model clearly fits the later stage of the process than it does the beginning. This difference is made even clearer when observing the residuals Figure 4.13. A clear trend or behavior can be observed at 15 minutes but at 60 minutes the residuals can be considered to have a completely normal random distribution. This difference is because in the model, the fouling layer has a preset thickness that when paired with the initial thermal conductivity, causes the model to not be able to heat up as fast as the experiment does. However, the overshooting of the model at the last 1 – 2 seconds was due to a preset outward convective heat flux value of $400 \text{ W/m}^2\text{K}$ when our estimates have shown it to be more in the vicinity of $\sim 500 \text{ W/m}^2\text{K}$. This higher value would mean a faster removal of heat from the sensor into the ambient which would result in the observed experimental curve.

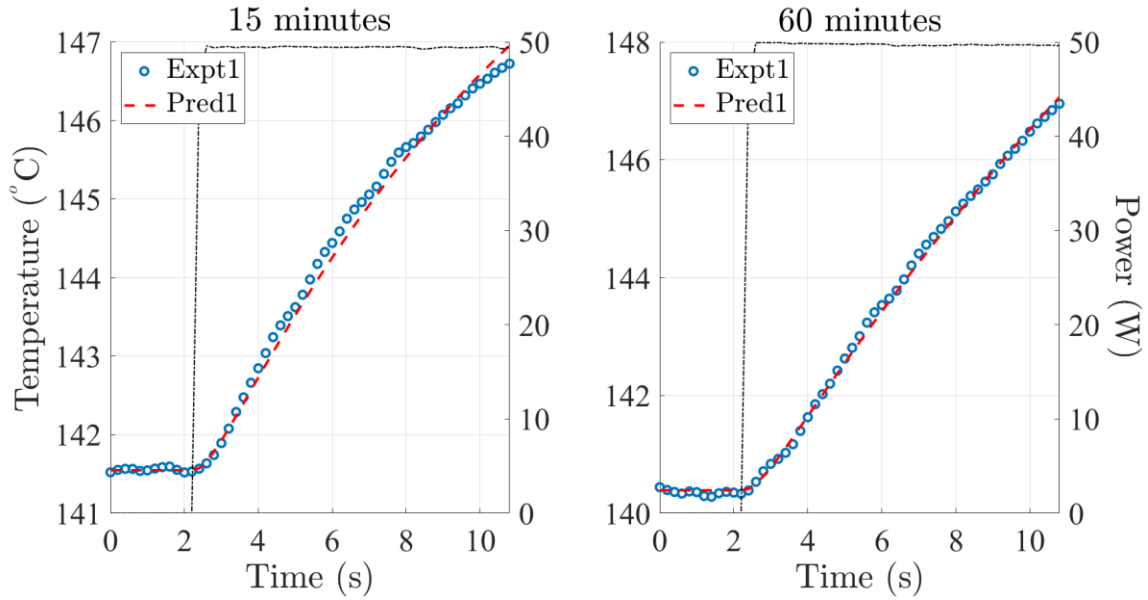


Figure 4.12. Temperature profile for the sensor heat pulse at 15 and 60 minutes of processing HWC.

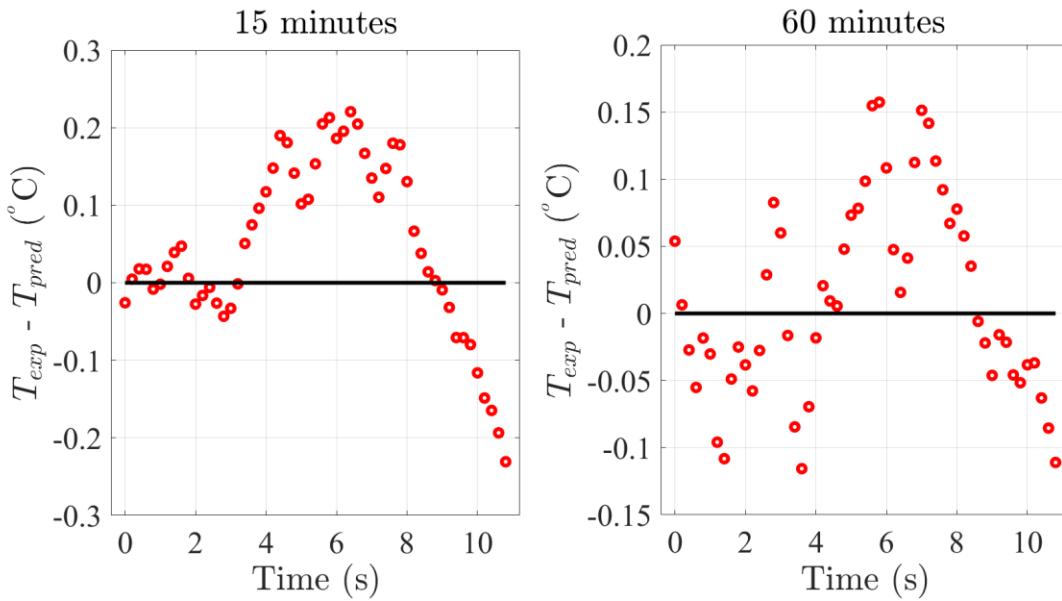


Figure 4.13. Residual plots for HWC temperature profile at 15 and 60 minutes of processing

The average thermal conductivity of NFDM and HWC are shown in Figure 4.14 and Figure 4.15, respectively. Values are plotted from the 15-minute mark because it takes the system approximately 10 minutes to stabilize once recirculation has started. Initial estimates of thermal

conductivity for the fouling layer are in accordance to values found in literature for both products since very little or no fouling is present at this moment. Chaves & De Almeida (2009) reported cream values (40% fat) to have a thermal conductivity of 0.42 W/(m·K) at 30 °C. Hayes (1987) reported thermal conductivity for cream (40% fat) to be 0.33 W/(m·K) and a previous study had reported cream (39.52% fat) to have a thermal conductivity of 0.3684 W/(m·K) at 80 °C (Martin & Montes, 1977). Choi & Okos (1986) predictive model for at 140 °C using composition values from Hu et al. (2009) gives a value of 0.33 W/(m·K) for HWC and 0.63 W/(m·K) for NFDM. Other values for NFDM have been presented in the previous section. The errors are increasing as time progresses. We know that the SSCs for both products are lower as time goes on which explains why our estimates would have larger errors further down the experiment. Also, the model used in this study has a preset thickness for the fouling layer of 0.5 mm when experimentally layers of 1.78 ± 0.30 and 1.65 ± 0.24 were observed for HWC and 15% NFDM. This would cause some uncertainty around the estimates as more fouling builds up.

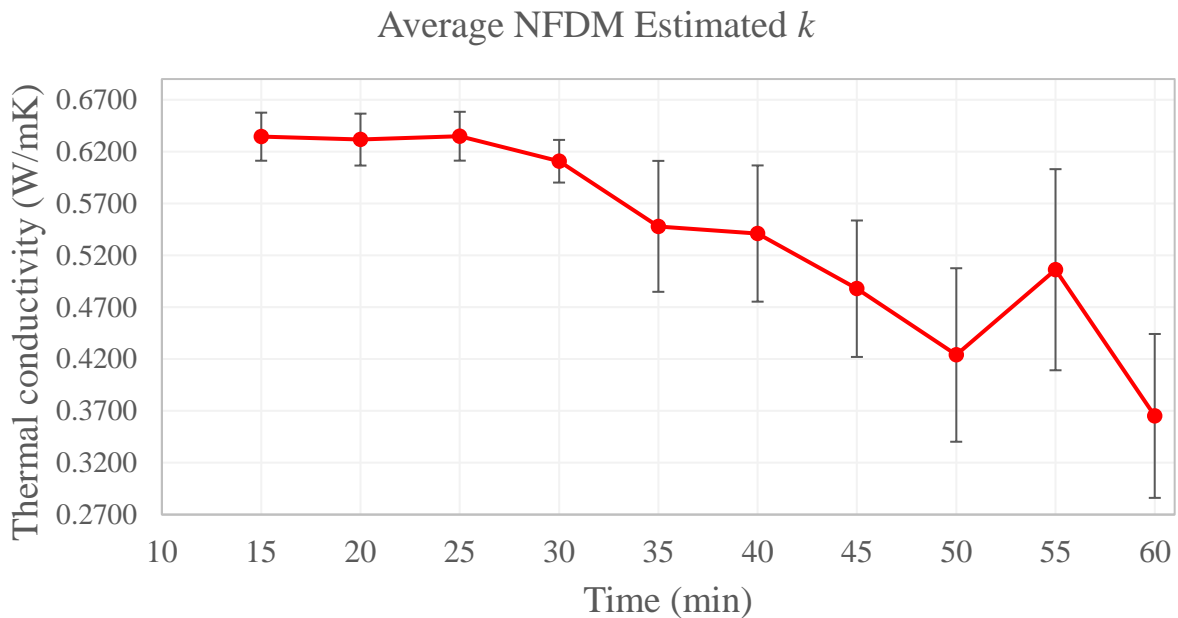


Figure 4.14. Estimated k average with 95% confidence interval for NFDM trials.

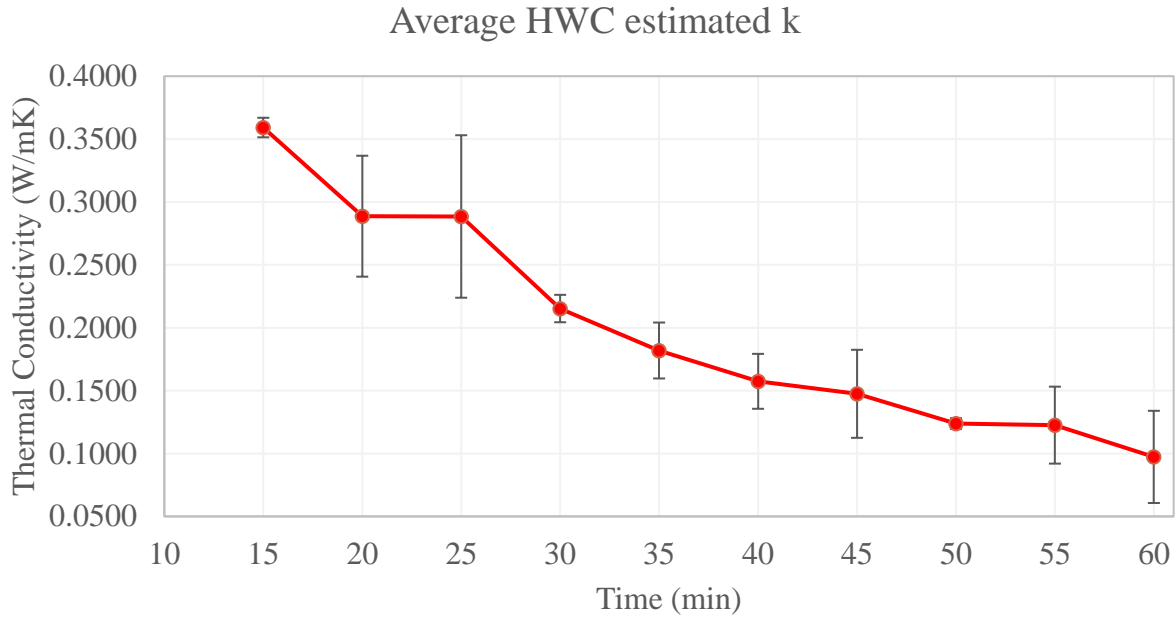


Figure 4.15. Estimated k average with 95% confidence interval for HWC trials.

A clear downward trend can be seen in Figure 4.14 and Figure 4.15 for the evolution of thermal conductivity as process time progresses. This can clearly be attributable to the formation of the fouling layer. Kazi et al. (2015) demonstrated this by proving how prolonged processing times reduced the overall heat transfer coefficient drastically because of fouling formation. Their study comprehended a much longer processing time, however, their process was single pass and the experiments here were recirculating.

Due to the high temperatures, the composition of the fouling layer can be considered to be mostly CaCO_3 deposits (Thamaraiselvan & Noel, 2015). Awad (2011) reported thermal conductivity of CaCO_3 to be $2.19 \text{ W}/(\text{m}\cdot\text{K})$, thus explaining why the estimated values would show a downward trend trying to reach this value. However, Hagsten et al. (2016) explained how the CaCO_3 deposits would most likely be closer to the stainless steel surface while the part closest to

the bulk would be mostly denatured protein. Since run times are limited to 1-hour trials, it could be said that the composition of the observed fouling layers is mostly CaCO_3 . Nevertheless, a compositional analysis is recommended to understand the properties of this layer completely.

Literature shows that fouling formation tends to have an asymptotic growth eventually reaching a stable value where both deposition and resuspension rates balance each other out (Prakash et al., 2005; Tuoc, 2015). This might not be as apparent in the NFDM trials but could explain the behavior of the HWC trials. Perhaps the NFDM fouling layer would require a longer time to reach this equilibrium.

4.5 Fouling Layer Image Analysis **EQUATION CHAPTER 4 SECTION 5**

An interactive interface was created in MATLAB that displays certain prompts to guide the user for data processing. A photo of the fouled tube was analyzed after every processing trial of NFDM and HWC (Figure 4.16). Original photo was cropped and zoomed in (Figure 4.17a) to be able to measure the thickness of the observed fouling layer.

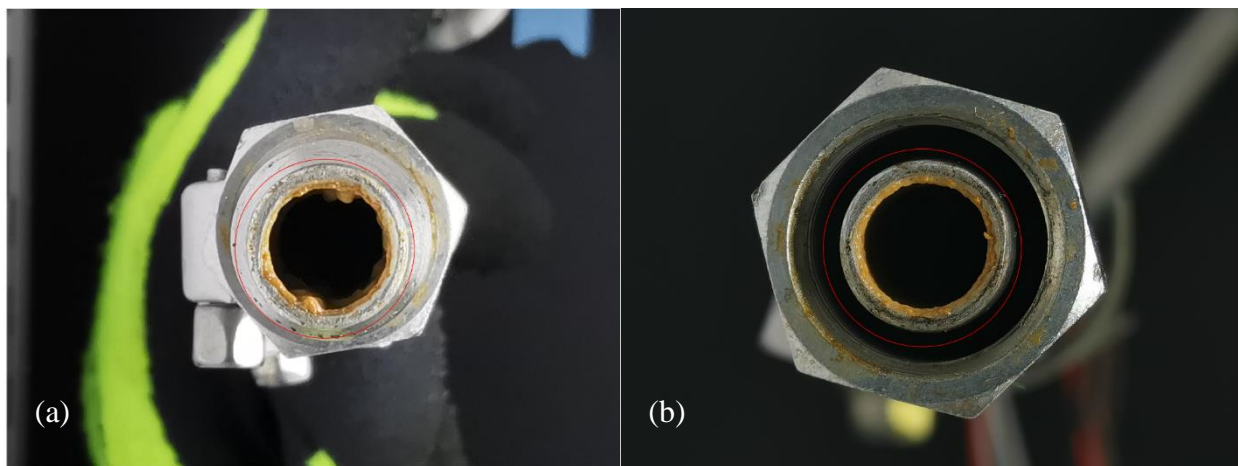


Figure 4.16. Photo of a fouled tube section mounted with NICS after (a) HWC trial and (b) NFDM trial

The code allows for multiple regions of interest (ROI) to be drawn as lines and displaying their distances within the image in pixels. 5 different sections of the fouling layer were selected to obtain comprehensive data on the fouling layer that had formed. Once these selections had been made, the pipe wall was measured and its distance in pixels was used as a reference distance to convert from pixels to millimeters (Figure 4.17).

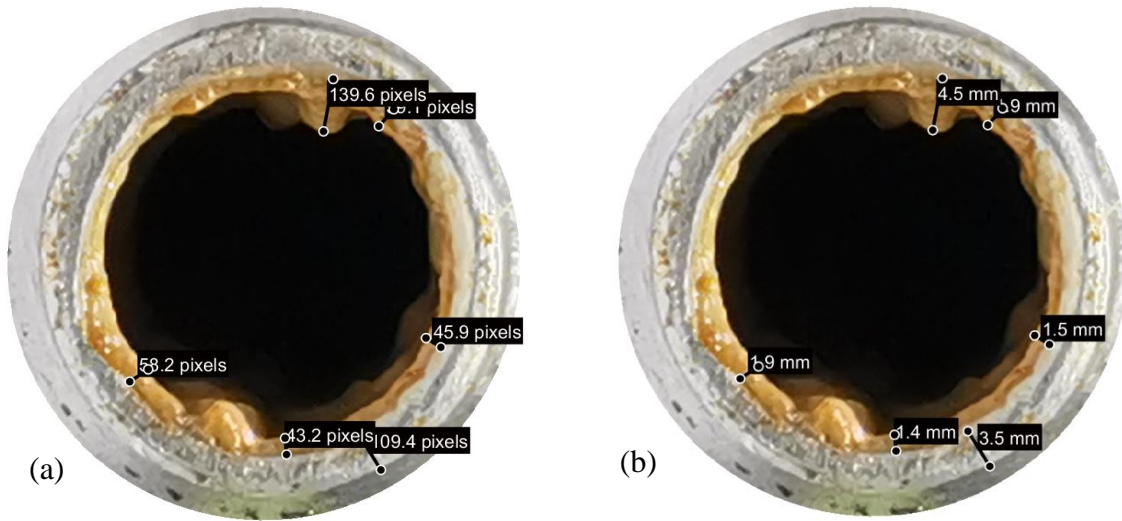


Figure 4.17.(a) ROI lines measuring pixels and scaling factor window (b) ROI lines measurements converted into corresponding units.

Figure 4.17a shows a fouled tube after an HWC trial where there seems to be no symmetry in the formation of the fouling layer. NFDM trials do not show this behavior and the differences are clearer when comparing the thermal resistance of both products (Figure 4.16b). Srichantra et al. (2006) studied the fouling rates of reconstituted and recombined (i.e. skim milk + milk fat) and reported that skim milk had higher fouling rates than its higher fat counterpart. This might explain why the fouling layer from processing HWC has no apparent pattern.

To calculate the thermal resistance of the fouling layer at the end of the trial, the thickness of the different sections of fouling were paired with the estimated thermal conductivity at the 60-minute mark of the process for both products. Thermal resistance was calculated by:

$$R_f = \frac{x_f}{k_f} \quad [4.5.1]$$

Where R_f is the thermal resistance of the fouling layer in $(\text{m}^2 \cdot \text{K})/\text{W}$, x_f is the thickness of the fouling layer evaluated at every ROI in meters and k_f is the estimated thermal conductivity of the fouling layer in $\text{W}/(\text{m} \cdot \text{K})$. The mean thickness and resistance for the fouling layer created after processing both products are shown in Table 4.2 with their corresponding standard deviations.

Table 4.2. Average thickness and thermal resistance of the fouling layer for HWC and 15% NFDM

Product	Thickness (mm)	Thermal Resistance $((\text{m}^2\text{K})/\text{W})$
HWC	1.78 ± 0.30	0.0260 ± 0.0119
15% NFDM	1.65 ± 0.24	0.0040 ± 0.0002

The larger standard deviation in the HWC thickness and thermal resistance further demonstrates how the formation of fouling is more random than in the NFDM trials. Bouvier et al. (2018) and Davies et al. (1997) both studied the thermal resistance of whey protein deposits by using heat flux sensors and reported values close to $1.0\text{E-}3 (\text{m}^2 \cdot \text{K})/\text{W}$ at about half the processing time used for this study. Since the thickness measured was higher than the simulation preset value, the estimated thermal conductivity values should be lower than real values. This would mean that real values for the thermal resistance would be lower than those reported, thereby it would be closer to those found in the literature.

CHAPTER 5. CONCLUSIONS AND FUTURE WORK

Correct implementation of sequential estimation allowed the sensor to determine the thermal conductivity of water, 4% starch solution, and 10% NFDM at 140 °C and of the fouling layer in HWC and 15% NFDM trials. The estimated thermal conductivities of the products were in accordance with literature. Overall, the fouling thermal conductivity was determined to have a decreasing trend as more fouling builds up. This build up was verified through image analysis which is a powerful tool that combined with the sensor can deepen our understanding of fouling formation. This will greatly aid the dairy industry in monitoring and detecting fouling to optimize their process and reduce their losses.

To obtain the best quality data and correctly implement sequential estimation, optimal experimental design and scaled sensitivity coefficients were presented for the measurement of thermal properties under food processing conditions. The information provided by the optimal experimental design was crucial in the design of NICS since every experiment was to be made in-line and the highest quality data was obtained in a matter of seconds.

The estimation process used in this study can be extended to estimate other parameters such as the convective heat flux that was estimated before estimating the thermal conductivity. The sensor's ability to estimate thermal conductivity can be applied to different products with considerable accuracy and precision apart from easy installation. NICS has the capability of being programmed to provide different configurations of heat pulses for optimal design based on product needs. The sensor is flexible enough to be placed anywhere in the system and estimate the thermal properties of the product as it passes through different stages of the process, opening the possibilities for future applications. This sensor will allow food industries to optimally design and engineer their processes by using high-quality thermal conductivity estimates.

Future work for this sensor is to first improve on the sensor design by adding an insulation layer to the outer surface of the sensor and add another thermocouple to avoid estimation of the heat transfer coefficient. Also, improve the model by applying a moving boundary condition to simulate fouling layer growth instead of having a fixed value of layer thickness in the model. Then use the estimation process to estimate fouling growth/deposition and resuspension rates. Sensor can then be used for other high protein products, especially plant-based protein to compare against animal protein.

APPENDIX A. TYPICAL RAW EXPERIMENTAL DATA FILE

Time (s)	Voltage (V)	Current (A)	Power (W)	Product In (°C)	Heater 1 Out (°C)	Heater 2 Out (°C)	Holding Tube Out (°C)	Cooling Out (°C)	Circulating Hot Water (°C)	Incoming Steam (°C)	NICS TC1 (°C)	NICS TC2 (°C)
0.00	0.01	0.00	0.00	28.47	95.39	150.34	140.11	27.99	94.61	153.04	142.31	142.19
0.20	0.01	0.00	0.00	28.38	95.33	150.30	139.98	28.01	94.71	152.93	142.24	142.10
0.40	0.01	0.00	0.00	28.33	95.32	150.33	140.11	28.27	94.63	153.04	142.26	142.13
0.60	0.01	0.00	0.00	28.32	95.25	150.25	140.07	28.41	94.67	152.93	142.31	142.06
0.80	0.01	0.00	0.00	28.35	95.25	150.32	140.11	28.59	94.73	152.98	142.25	142.13
1.00	0.01	0.00	0.00	28.44	95.21	150.43	140.22	28.79	94.66	153.00	142.33	142.13
1.20	0.01	0.00	0.00	28.39	95.32	150.34	140.21	28.94	94.83	152.98	142.30	142.17
1.40	0.01	0.00	0.00	28.32	95.25	150.32	140.09	28.82	94.69	152.92	142.23	142.07
1.60	0.01	0.00	0.00	28.39	95.27	150.28	140.08	28.88	94.69	153.00	142.25	141.99
1.80	0.01	0.00	0.00	28.54	95.37	150.42	140.20	28.70	94.75	153.03	142.25	142.14
2.00	0.01	0.00	0.00	28.39	95.31	150.34	140.14	28.55	94.80	153.02	142.34	142.13
2.20	0.01	0.00	0.00	28.42	95.20	150.23	140.09	28.11	94.73	152.95	142.11	142.05
2.40	28.38	1.66	47.16	28.46	95.29	150.27	140.31	27.91	94.69	153.01	142.27	142.13
2.60	29.64	1.73	51.41	28.48	95.35	150.37	140.28	27.65	94.90	153.07	142.37	142.33
2.80	29.60	1.73	51.25	28.44	95.32	150.36	140.17	27.54	94.83	153.10	142.20	142.52
3.00	29.61	1.73	51.24	28.49	95.29	150.42	140.23	27.45	94.88	153.09	142.44	142.79
3.20	29.59	1.73	51.16	28.56	95.22	150.46	140.21	27.47	94.87	153.12	142.57	143.09
3.40	29.62	1.73	51.15	28.54	95.34	150.38	140.26	27.47	94.81	153.21	142.80	143.28
3.60	29.62	1.73	51.16	28.40	95.31	150.37	140.14	27.61	94.80	153.14	142.94	143.57
3.80	29.58	1.72	51.02	28.47	95.25	150.26	140.17	27.72	94.74	153.04	143.16	143.62
4.00	29.62	1.73	51.15	28.44	95.25	150.37	140.05	27.79	94.78	153.03	143.36	143.94
4.20	29.62	1.73	51.11	28.41	95.22	150.34	140.06	27.90	94.83	153.11	143.59	144.22
4.40	29.62	1.73	51.12	28.51	95.15	150.27	140.02	27.73	94.70	153.06	143.76	144.32
4.60	29.62	1.73	51.12	28.45	95.26	150.31	140.18	27.73	94.87	153.02	143.98	144.47
4.80	29.63	1.73	51.15	28.45	95.20	150.32	140.07	27.74	94.83	153.08	144.21	144.66
5.00	29.64	1.73	51.18	28.52	95.15	150.39	140.18	27.74	94.94	152.99	144.36	144.89
5.20	29.63	1.73	51.14	28.52	95.28	150.48	140.21	28.01	94.88	153.15	144.70	145.21
5.40	29.63	1.73	51.16	28.51	95.23	150.34	140.04	27.63	94.90	153.04	144.88	145.27
5.60	29.60	1.73	51.07	28.49	95.25	150.44	140.20	27.75	94.91	153.05	145.08	145.47
5.80	29.63	1.73	51.15	28.37	95.10	150.36	140.05	27.60	94.78	152.94	145.25	145.62
6.00	29.63	1.73	51.16	28.46	95.22	150.33	140.13	27.70	94.77	152.95	145.55	145.89
6.20	29.62	1.73	51.13	28.31	95.16	150.29	140.06	27.74	94.75	152.94	145.66	145.94
6.40	29.62	1.73	51.10	28.33	95.11	150.31	140.03	27.80	94.86	153.03	145.90	146.26
6.60	29.63	1.73	51.12	28.46	95.19	150.38	140.09	27.88	94.88	152.96	146.05	146.28
6.80	29.60	1.72	51.03	28.37	95.19	150.34	140.11	27.70	94.68	152.97	146.16	146.40
7.00	29.63	1.73	51.12	28.51	95.20	150.42	140.02	28.00	94.82	153.09	146.41	146.62

Continued

Appendix A continued

7.20	29.63	1.72	51.10	28.50	95.21	150.39	140.06	28.21	94.80	153.07	146.62	146.78
7.40	29.56	1.72	50.85	28.51	95.20	150.40	140.12	28.19	94.75	153.05	146.73	147.01
7.60	29.62	1.72	51.08	28.57	95.43	150.45	140.12	28.47	94.90	153.14	146.96	147.16
7.80	29.63	1.72	51.11	28.32	95.11	150.30	139.96	28.21	94.77	153.01	146.85	147.23
8.00	29.60	1.72	51.00	28.38	95.15	150.37	140.05	28.06	94.78	153.00	147.11	147.31
8.20	29.62	1.72	51.02	28.57	95.19	150.41	140.17	28.09	94.69	152.98	147.23	147.54
8.40	29.63	1.72	51.05	28.42	95.04	150.33	140.05	28.03	94.75	152.94	147.23	147.51
8.60	29.62	1.72	51.02	28.49	95.12	150.48	140.10	28.24	94.81	153.08	147.44	147.73
8.80	29.64	1.72	51.07	28.44	95.07	150.39	140.03	28.43	94.79	153.01	147.57	147.78
9.00	29.64	1.72	51.10	28.48	95.13	150.43	140.13	28.60	94.90	153.08	147.86	147.86
9.20	29.64	1.72	51.09	28.40	95.09	150.37	140.05	28.52	94.79	153.02	147.86	147.94
9.40	29.64	1.72	51.08	28.37	95.07	150.34	140.06	28.52	94.90	153.03	147.99	148.05
9.60	29.63	1.72	51.03	28.40	95.02	150.45	140.11	28.61	94.79	153.05	148.08	148.20
9.80	29.63	1.72	51.02	28.49	95.15	150.45	140.04	28.74	94.84	153.07	148.31	148.33
10.00	29.63	1.72	51.03	28.41	95.10	150.39	140.08	28.57	94.86	153.05	148.46	148.46
10.20	29.63	1.72	51.04	28.39	95.12	150.43	139.95	28.40	94.83	153.00	148.45	148.56
10.40	29.62	1.72	50.97	28.53	95.20	150.47	140.17	28.45	94.90	153.10	148.71	148.72
10.60	29.61	1.72	50.94	28.55	95.10	150.45	140.10	28.11	94.74	152.98	148.68	148.76
10.80	29.62	1.72	50.97	28.54	95.13	150.52	140.09	27.94	94.81	153.05	148.78	148.89
11.00	29.61	1.72	50.94	28.42	95.07	150.44	140.08	28.02	94.79	152.93	148.96	149.02
11.20	29.62	1.72	50.93	28.45	95.05	150.41	139.98	28.04	94.72	152.97	149.04	149.02
11.40	29.60	1.72	50.90	28.42	95.03	150.42	140.09	28.11	94.72	153.06	149.09	149.18
11.60	29.61	1.72	50.92	28.61	95.16	150.53	140.09	28.25	94.94	153.11	149.32	149.28
11.80	29.61	1.72	50.93	28.53	95.16	150.39	140.05	28.17	94.82	153.01	149.41	149.40
12.00	29.62	1.72	50.88	28.41	95.11	150.50	140.13	28.01	94.84	153.01	149.56	149.46
12.20	29.60	1.72	50.88	28.37	95.08	150.49	140.04	27.68	94.77	153.04	149.51	149.55
12.40	29.62	1.72	50.95	28.62	95.25	150.52	140.26	27.70	94.95	153.13	149.72	149.81
12.60	29.61	1.72	50.91	28.50	94.95	150.42	140.13	27.43	94.85	152.95	149.60	149.73
12.80	29.57	1.72	50.74	28.54	95.04	150.47	140.13	27.41	94.90	153.07	149.78	149.88
13.00	29.59	1.72	50.83	28.55	95.07	150.49	140.11	27.44	94.90	153.08	149.96	149.93
13.20	29.61	1.72	50.88	28.41	94.98	150.38	140.03	27.55	94.74	152.99	150.06	150.04
13.40	29.63	1.72	50.91	28.39	94.99	150.42	140.13	27.93	94.81	152.98	150.16	150.11
13.60	29.63	1.72	50.95	28.45	95.03	150.41	140.09	28.12	94.78	153.02	150.21	150.25
13.80	29.63	1.72	50.96	28.50	94.96	150.39	139.99	28.25	94.79	153.01	150.23	150.21
14.00	29.62	1.72	50.92	28.46	95.06	150.50	140.13	28.34	94.92	153.00	150.41	150.44
14.20	29.64	1.72	50.98	28.37	94.96	150.37	140.09	28.28	94.75	153.02	150.48	150.42
14.40	29.62	1.72	50.88	28.54	95.11	150.50	140.19	28.42	94.83	153.03	150.67	150.58
14.60	29.63	1.72	50.93	28.43	95.03	150.46	140.16	28.45	94.80	153.00	150.64	150.57
14.80	29.57	1.71	50.64	28.41	94.98	150.44	140.11	28.24	94.78	153.03	150.74	150.72
15.00	29.62	1.72	50.85	28.40	95.02	150.46	140.12	27.83	94.80	152.99	150.79	150.74
15.20	29.58	1.72	50.74	28.35	94.97	150.33	139.96	27.52	94.70	152.98	150.83	150.76
15.40	29.65	1.72	50.98	28.49	95.01	150.51	140.24	27.52	94.77	153.13	150.95	150.99

Continued

Appendix A continued

15.60	29.60	1.72	50.81	28.38	95.05	150.49	140.26	27.33	94.72	153.00	151.00	151.01
15.80	29.64	1.72	50.92	28.49	94.99	150.41	140.17	27.20	94.62	153.01	151.09	150.97
16.00	29.64	1.72	50.92	28.42	94.98	150.49	140.16	27.15	94.65	152.98	151.10	151.06
16.20	29.64	1.72	50.91	28.37	95.09	150.55	140.25	27.26	94.70	152.97	151.16	151.16
16.40	29.65	1.72	50.93	28.46	95.11	150.54	140.25	27.47	94.75	153.01	151.36	151.20
16.60	29.66	1.72	51.00	28.45	95.05	150.43	140.15	27.63	94.59	153.08	151.35	151.25
16.80	29.63	1.72	50.90	28.52	94.98	150.44	140.21	27.85	94.79	153.06	151.47	151.32
17.00	29.62	1.72	50.88	28.31	94.92	150.38	140.13	27.96	94.56	152.91	151.50	151.38
17.20	8.55	0.50	4.24	28.33	95.02	150.44	140.18	28.16	94.70	153.01	151.62	151.51
17.40	0.01	0.00	0.00	28.40	95.05	150.47	140.14	28.49	94.72	153.02	151.71	151.52
17.60	0.01	0.00	0.00	28.38	95.03	150.58	140.27	28.71	94.79	152.96	151.72	151.32
17.80	0.01	0.00	0.00	28.23	95.00	150.41	140.18	28.53	94.71	152.99	151.66	151.07
18.00	0.01	0.00	0.00	28.26	95.05	150.42	140.21	28.59	94.58	153.02	151.56	150.80

REFERENCES

- Awad, M. M. (2011). *Fouling of Heat Transfer Surfaces*. <https://doi.org/10.5772/13696>
- AZO Materials. (2001). *Stainless Steel - Grade 316 (UNS S31600)*. <https://www.azom.com/article.aspx?ArticleID=863>
- Bansal, B., & Chen, X. D. (2006). A Critical Review of Milk Fouling in Heat Exchangers. *Comprehensive Reviews in Food Science and Food Safety*, 5(2), 27–33. <https://doi.org/10.1111/j.1541-4337.2006.tb00080.x>
- Beck, J. V., & Arnold, K. J. (1977). *Parameter Estimation in Engineering and Science*. John Wiley & Sons, Inc.
- Beck, J. V., Blackwell, B., & St. Clair, C. R. J. (1985). *Inverse Heat Conduction: Ill-Posed Problems*. John Wiley & Sons, Inc. https://books.google.com/books?hl=en&lr=&id=-1hzLAb_ZL0C&oi=fnd&pg=PR15&ots=i_gtHOd_-j&sig=DPhIYIJ14gqLply0x7ybmc7Ssvg#v=onepage&q&f=true
- Bluma, A., Höpfner, T., Lindner, P., Rehbock, C., Beutel, S., Riechers, D., Hitzmann, B., & Scheper, T. (2010). In-situ imaging sensors for bioprocess monitoring: state of the art. *Analytical and Bioanalytical Chemistry*, 398(6), 2429–2438. <https://doi.org/10.1007/s00216-010-4181-y>
- Bott, T. R. (1995). Basic Principles. In T. R. BOTT (Ed.), *Fouling of Heat Exchangers* (pp. 7–14). Elsevier. <https://doi.org/10.1016/B978-044482186-7/50004-X>
- Bouvier, L., Delaplace, G., & Lalot, S. (2018). Continuous Monitoring of Whey Protein Fouling Using a Nonintrusive Sensor. *Heat Transfer Engineering*, 1–26. <https://doi.org/10.1080/01457632.2018.1522091>
- Buhri, A. B., & Singh, R. P. (1993). Measurement of Food Thermal Conductivity Using Differential Scanning Calorimetry. *Journal of Food Science*, 58(5), 1145–1147. <https://doi.org/10.1111/j.1365-2621.1993.tb06134.x>
- Cardarelli, F. (2008). Ferrous Metals and Their Alloys. In *Materials Handbook* (pp. 59–157). Springer London. https://doi.org/10.1007/978-1-84628-669-8_2
- Caruyer, C., Minier, J., Guingo, M., & Henry, C. (2016). A Stochastic Model for Particle Deposition in Turbulent Flows and Clogging Effects (pp. 451–466). https://doi.org/10.1007/978-981-287-615-7_31

- Cattani, F., Dolan, K. D., Oliveira, S. D., Mishra, D. K., Ferreira, C. A. S., Periago, P. M., Aznar, A., Fernandez, P. S., & Valdramidis, V. P. (2016). One-step global parameter estimation of kinetic inactivation parameters for *Bacillus sporothermodurans* spores under static and dynamic thermal processes. *Food Research International*, 89, 614–619. <https://doi.org/https://doi.org/10.1016/j.foodres.2016.08.027>
- Chan, J. P., & Batchelor, B. G. (1993). Machine vision for the food industry. In *Food Process Monitoring Systems I* (p. 44).
- Chaves, M. A., & De Almeida, A. O. (2009). Development of a Microcontrolled Instrument to Determinate Thermal Conductivity of Foods. In *International Journal of Food Engineering* (Vol. 5). <https://doi.org/10.2202/1556-3758.1710>
- Choi, Y., & Okos, M. R. (1986). Thermal properties of liquid foods - review [Article]. *ASAE Publication*, 35–77.
- Coker, A. K. (2007). *Physical properties of liquids and gases* (A. K. B. T.-L. A. P. D. for C. and P. P. (Fourth E. Coker (ed.); pp. 103–132). Gulf Professional Publishing. <https://doi.org/https://doi.org/10.1016/B978-075067766-0/50010-5>
- COMSOL. (2018). *COMSOL Multiphysics* (5.4). COMSOL Inc.
- Crattelet, J., Ghnimi, S., Debreyne, P., Zaid, I., Boukabache, A., Esteve, D., Auret, L., & Fillaudeau, L. (2013). On-line local thermal pulse analysis sensor to monitor fouling and cleaning: Application to dairy product pasteurisation with an ohmic cell jet heater. *Journal of Food Engineering*, 119(1), 72–83. <https://doi.org/10.1016/J.JFOODENG.2013.05.009>
- D'Alessandro, G., & de Monte, F. (2017). Sensitivity coefficients for thermal properties measurements using a boundary condition of the 4 th kind. *Journal of Physics: Conference Series*, 796, 012011. <https://doi.org/10.1088/1742-6596/796/1/012011>
- David, J. R. D., Graves, R. H., & Szemplenski, T. (2012). *Handbook of Aseptic Processing and Packaging*. CRC Press. <https://doi.org/10.1201/b13026>
- Davies, T. J., Henstridge, S. C., Gillham, C. R., & Wilson, D. I. (1997). Investigation of Whey Protein Deposit Properties Using Heat Flux Sensors. *Food and Bioproducts Processing*, 75(2), 106–110. <https://doi.org/https://doi.org/10.1205/096030897531414>
- Dolan, K. D., & Mishra, D. K. (2013). *Parameter Estimation in Food Science*. <https://doi.org/10.1146/annurev-food-022811-101247>
- Feidt, M. (2017). *1 - From Thermostatistics to Non-equilibrium Thermodynamics* (M. B. T.-F. P. D.

- O. T. 1 Feidt (ed.); pp. 1–41). Elsevier. <https://doi.org/https://doi.org/10.1016/B978-1-78548-232-8.50001-7>
- FSIS, U. (2014). *Shelf-Stable Food Safety*. https://www.fsis.usda.gov/wps/wcm/connect/77ffde83-dc51-4fdf-93be-048110fe47d6/Shelf_Stable_Food_Safety.pdf?MOD=AJPERES
- Gillham, C. R., Fryer, P. J., Hasting, A. P. M., & Wilson, D. I. (1999). Cleaning-in-Place of Whey Protein Fouling Deposits: Mechanisms Controlling Cleaning. *Food and Bioprocess Technology*, 77(2), 127–136. <https://doi.org/10.1205/096030899532420>
- Gratzek, J. P., & Toledo, R. T. (1993). Solid Food Thermal Conductivity Determination at High Temperatures. *Journal of Food Science*, 58(4), 908–913. <https://doi.org/10.1111/j.1365-2621.1993.tb09389.x>
- Greiby, I., Mishra, D. K., & Dolan, K. D. (2014). Inverse method to sequentially estimate temperature-dependent thermal conductivity of cherry pomace during nonisothermal heating. *Journal of Food Engineering*, 127, 16–23. <https://doi.org/10.1016/J.JFOODENG.2013.10.039>
- Gudmundsson, O., Palsson, O. P., Palsson, H., & Lalot, S. (2016). Online Fouling Detection of Domestic Hot Water Heat Exchangers. *Heat Transfer Engineering*, 37(15), 1231–1241. <https://doi.org/10.1080/01457632.2015.1119584>
- Gustafsson, S. E., Karawacki, E., & Khan, M. N. (1979). Transient hot-strip method for simultaneously measuring thermal conductivity and thermal diffusivity of solids and fluids. *Journal of Physics D: Applied Physics*, 12(9), 1411–1421. <https://doi.org/10.1088/0022-3727/12/9/003>
- Hagsten, C., Altskär, A., Gustafsson, S., Lorén, N., Hamberg, L., Innings, F., Paulsson, M., & Nylander, T. (2016). Composition and structure of high temperature dairy fouling. *Food Structure*, 7, 13–20. <https://doi.org/https://doi.org/10.1016/j.foostr.2015.12.002>
- Hayes, G. D. (1987). *Food Engineering Data Handbook*. Harlow, Essex, England : Longman Scientific & Technical ; New York : Wiley. <https://trove.nla.gov.au/work/12550858?q&versionId=45427996>
- Ho, C. Y., Powell, R. W., & Liley, P. E. (1968). Thermal Conductivity of Selected Materials, Part 2. *Nsrds-Nbs 16*, 168.
- Hu, J., Sari, O., Eicher, S., & Rija Rakotozanakajy, A. (2009). Determination of specific heat of

- milk at different fat content between 1 °C and 59 °C using micro DSC. *Journal of Food Engineering*, 90(3), 395–399. <https://doi.org/10.1016/J.JFOODENG.2008.07.009>
- Ibrahim, H. (2012). Fouling in Heat Exchangers. In V. N. Katsikis (Ed.), *MATLAB - A fundamental tool for scientific computing and engineering applications* (Vol. 3). IntechOpen. <https://doi.org/10.5772/46462>
- Jewell, K. (2012). Comparison of 1-step and 2-step methods of fitting microbiological models. *International Journal of Food Microbiology*, 160(2), 145–161. <https://doi.org/https://doi.org/10.1016/j.ijfoodmicro.2012.09.017>
- Kazi, S. N., Teng, K. H., Zakaria, M. S., Sadeghinezhad, E., & Bakar, M. A. (2015). Study of mineral fouling mitigation on heat exchanger surface. *Desalination*, 367, 248–254. <https://doi.org/https://doi.org/10.1016/j.desal.2015.04.011>
- Lewis, M. J. (2000). *Continuous thermal processing of foods: pasteurization and UHT sterilization* (N. J. Heppell (ed.)). Aspen Publishers.
- Lloyd, I. K., Kolos, K. R., Menegaux, E. C., Luo, H., McCuen, R. H., & Regan, T. M. (1995). *Structure, processing and properties of potatoes*. <https://ntrs.nasa.gov/search.jsp?R=19920021045>
- Mariani, V. C., Camargo Do Amarante, A. C., & Coelho, L. D. S. (2009). Estimation of apparent thermal conductivity of carrot puré e during freezing using inverse problem. *International Journal of Food Science & Technology*, 44, 1292–1303. <https://doi.org/10.1111/j.1365-2621.2009.01958.x>
- Martin, F. F., & Montes, F. (1977). Thermal conductivity of creams. *Journal of Dairy Research*, 44(1), 103–109. <https://doi.org/10.1017/S0022029900019993>
- May NS. (2001). Retort technology. In *Thermal technologies in food processing*. <https://doi.org/10.1533/9781855736610.1.5>
- McFarlane, I. (1995). In-line sensors. In I. McFarlane (Ed.), *Automatic Control of Food Manufacturing Proceses* (pp. 8–35). Springer US. https://doi.org/10.1007/978-1-4615-2187-7_2
- Mishra, D. K., Dolan, K. D., Beck, J. V., & Ozadali, F. (2016). A novel instrument for rapid measurement of temperature-dependent thermal properties of conduction-heated food up to 140 °C. *Journal of Food Engineering*, 191, 19–27. <https://doi.org/10.1016/J.JFOODENG.2016.06.028>

- Mishra, D. K., Dolan, K. D., Beck, J. V., & Lansing, E. (2009). Optimal Experimental Design to Estimate Thermal Degradation Kinetic Parameters for Nutraceuticals in Intermediate-Moisture Foods. *ASABE Annual International Meeting*, 9. <https://elibrary.asabe.org/pdfviewer.asp?param1=s:/8y9u8/q8qu/tq9q/5tv/L/7u34IGGP/GPMLKL.5tv¶m2=HI/K/IGHP¶m3=HIO.IHG.HII.IGH¶m4=27153>
- Mishra, D. K., Dolan, K. D., Beck, J. V., & Ozadali, F. (2017). Use of Scaled Sensitivity Coefficient Relations for Intrinsic Verification of Numerical Codes and Parameter Estimation for Heat Conduction. *Journal of Verification, Validation and Uncertainty Quantification*, 2(3). <https://doi.org/10.1115/1.4038494>
- Mohamed, I. O. (2009). Simultaneous estimation of thermal conductivity and volumetric heat capacity for solid foods using sequential parameter estimation technique. *Food Research International*, 42(2), 231–236. <https://doi.org/https://doi.org/10.1016/j.foodres.2008.11.002>
- Monteau, J.-Y. (2008). Estimation of thermal conductivity of sandwich bread using an inverse method. *Journal of Food Engineering*, 85(1), 132–140. <https://doi.org/10.1016/J.JFOODENG.2007.04.034>
- Muramatsu, Y., Greiby, I., Mishra, D. K., & Dolan, K. D. (2017). Rapid Inverse Method to Measure Thermal Diffusivity of Low-Moisture Foods. *Journal of Food Science*, 82(2), 420–428. <https://doi.org/10.1111/1750-3841.13563>
- Peleg, M., Normand, M. D., & Campanella, O. H. (2003). Estimating microbial inactivation parameters from survival curves obtained under varying conditions—The linear case. *Bulletin of Mathematical Biology*, 65(2), 219–234. [https://doi.org/10.1016/S0092-8240\(02\)00097-6](https://doi.org/10.1016/S0092-8240(02)00097-6)
- Pereira, C. G., De Resende, J. V., De Oliveira Giarola, T. M., Pinto, S. M., & De Abreu, L. R. (2013). Thermal conductivity of milk with different levels of moisture and fat: Experimental measures and prediction models. *Semina: Ciências Agrárias*, 34(3), 1153–1166. <https://doi.org/10.5433/1679-0359.2013v34n3p1153>
- Pinder, A. C., & Gatley, S. (1993). Fluorescence cytometry for the rapid analysis of food microorganisms. In *Food Process Monitoring Systems* (p. 28).
- Prakash, S., Datta, N., & Deeth, H. C. (2005). Methods of Detecting Fouling Caused by Heating of Milk. *Food Reviews International*, 21(3), 267–293. <https://doi.org/10.1080/FRI-200061609>
- Ramires, M. L. V., Nieto Castro, C. A., Nagasaka, Y., Nagashima, A., Assael, M. J., & Wakeham,

- W. A. (1995). Standard Reference Data for the Thermal Conductivity of Water. In *Journal of Physical and Chemical Reference Data* (Vol. 24, Issue 3, pp. 1377–1381). <https://doi.org/10.1063/1.555963>
- Rice, P., Selman, J. D., & Abdul-Rezzak, R. K. (2007). Effect of temperature on thermal properties of ‘Record’ potatoes. *International Journal of Food Science & Technology*, 23(3), 281–286. <https://doi.org/10.1111/j.1365-2621.1988.tb00580.x>
- Samsudin, H., Auras, R., Mishra, D., Dolan, K., Burgess, G., Rubino, M., Selke, S., & Soto-Valdez, H. (2018). Migration of antioxidants from polylactic acid films: A parameter estimation approach and an overview of the current mass transfer models. *Food Research International*, 103, 515–528. <https://doi.org/10.1016/J.FOODRES.2017.09.021>
- Saravacos, G., & Kostaropoulos, A. E. (2016). *Thermal Processing Equipment BT - Handbook of Food Processing Equipment* (G. Saravacos & A. E. Kostaropoulos (eds.); pp. 503–548). Springer International Publishing. https://doi.org/10.1007/978-3-319-25020-5_10
- Scheerlinck, N., Berhane, N. H., Moles, C. G., Banga, J. R., & Nicolai, B. M. (2008). Optimal dynamic heat generation profiles for simultaneous estimation of thermal food properties using a hotwire probe: Computation, implementation and validation. *Journal of Food Engineering*, 84(2), 297–306. <https://doi.org/10.1016/j.jfoodeng.2007.05.019>
- Schlüter, F., Augustin, W., & Scholl, S. (2019). Modeling local fouling resistances. *Heat Exchanger Fouling and Cleaning*, 10. [http://www.heatexchanger-fouling.com/papers/papers2019/03_Schlueter et al.pdf](http://www.heatexchanger-fouling.com/papers/papers2019/03_Schlueter%20et%20al.pdf)
- Shah, K. K., Tong, C. H., & Lund, D. B. (2000). Methodology to Obtain True Thermal Conductivity of Low Porosity Food Powders. *Journal of Food Science*, 65(6), 962–966. <https://doi.org/10.1111/j.1365-2621.2000.tb09400.x>
- Singh, A., Walvekar, R., Mohammad Khalid, Wong, W. Y., & Gupta, T. C. S. M. (2018). Thermophysical properties of glycerol and polyethylene glycol (PEG 600) based DES. *Journal of Molecular Liquids*, 252, 439–444. <https://doi.org/10.1016/j.molliq.2017.10.030>
- Srichantra, A., Newstead, D. F., McCarthy, O. J., & Paterson, A. H. J. (2006). Effect of Preheating on Fouling of a Pilot Scale UHT Sterilizing Plant by Recombined, Reconstituted and Fresh Whole Milks. *Food and Bioproducts Processing*, 84(4), 279–285. <https://doi.org/10.1205/FBP06027>

- Sulaiman, R., Dolan, K. D., & Mishra, D. K. (2012). Simultaneous and sequential estimation of kinetic parameters in a starch viscosity model. *Journal of Food Engineering*, 114(3), 313–322. <https://www.sciencedirect.com/science/article/abs/pii/S0260877412003998>
- Thamaraiselvan, C., & Noel, M. (2015). Membrane Processes for Dye Wastewater Treatment: Recent Progress in Fouling Control. *Critical Reviews in Environmental Science and Technology*, 45(10), 1007–1040. <https://doi.org/10.1080/10643389.2014.900242>
- Tuoc, T. K. (2015). *Chapter 20 - Fouling in Dairy Processes* (Z. Amjad & K. D. B. T.-M. S. and D. Demadis (eds.); pp. 533–556). Elsevier. <https://doi.org/https://doi.org/10.1016/B978-0-444-63228-9.00020-6>
- Verma, L. S., Singh, R., & Chaudhary, D. R. (1993). Probe controlled transient method for simultaneous determination of thermal conductivity and thermal diffusivity. *Journal of Physics D: Applied Physics*, 26(2), 259–270. <https://doi.org/10.1088/0022-3727/26/2/014>
- Wagner, W., & Kretzschmar, H.-J. (2007). *International Steam Tables : Properties of Water and Steam Based on the Industrial Formulation Iapws-If97 - Tables, Algorithms, Diagrams, and CD-ROM Electronic Steam Tables - All of the Equations of Iapws-If97 Including a Complete Set of Supplemen... Springer.*
<http://ebookcentral.proquest.com/lib/purdue/detail.action?docID=603571>
- Wallhäüßer, E., Hussein, M. A., & Becker, T. (2012). Detection methods of fouling in heat exchangers in the food industry. *Food Control*, 27, 1–10. <https://doi.org/10.1016/j.foodcont.2012.02.033>
- Wang, J., & Hayakawa, K. (1993). Thermal Conductivities of Starch Gels at High Temperatures Influenced by Moisture. *Journal of Food Science*, 58(4), 884–887. <https://doi.org/10.1111/j.1365-2621.1993.tb09383.x>
- Zhao, D., Qian, X., Gu, X., Jajja, S. A., & Yang, R. (2016). Measurement Techniques for Thermal Conductivity and Interfacial Thermal Conductance of Bulk and Thin Film Materials. *Journal of Electronic Packaging*, 138(4), 040802. <https://doi.org/10.1115/1.4034605>
- Zuoco, J., Alhama, F., & González Fernández, C. F. (2004). Inverse determination of the specific heat of foods. *Journal of Food Engineering*, 64(3), 347–353. <https://doi.org/10.1016/J.JFOODENG.2003.10.017>